Molecular Therapy
Oncolytics
Original Article

Exosomal and intracellular miR-320b promotes lymphatic metastasis in esophageal squamous cell carcinoma

Tong Liu,[1,5] Peilong Li,[1,2,5] Juan Li,[1,2,5] Qiuchen Qi,[1,2] Zhaowei Sun,[3] Shuang Shi,[1] Yan Xie,[1] Shibiao Liu,[1] Yunshan Wang,[1,2,4] Lutao Du,[1,2,4] and Chuanxin Wang[1,2,4]

[1]Department of Clinical Laboratory, The Second Hospital, Cheeloo College of Medicine, Shandong University, Jinan, Shandong 250033, China; [2]Shandong Engineering & Technology Research Center for Tumor Marker Detection, Jinan, Shandong, China; [3]Department of Surgery, The Affiliated Hospital of Medical College Qingdao University, Qingdao, China; [4]Shandong Provincial Clinical Medicine Research Center for Clinical Laboratory, Jinan, Shandong, China

Cancer-cell-released exosomal microRNAs (miRNAs) are important mediators of cell-cell communication in the tumor microenvironment. In this study, we sequenced serum exosome miRNAs from esophageal squamous cell carcinoma (ESCC) patients and identified high expression of miR-320b to be closely associated with peritumoral lymphangiogenesis and lymph node (LN) metastasis. Functionally, miR-320b could be enriched and transferred by ESCC-released exosomes directly to human lymphatic endothelial cells (HLECs), promoting tube formation and migration *in vitro* and facilitating lymphangiogenesis and LN metastasis *in vivo* as assessed by gain- and loss-of-function experiments. Furthermore, we found programmed cell death 4 (PDCD4) as a direct target of miR-320b through bioinformatic prediction and luciferase reporter assay. Re-expression of PDCD4 could rescue the effects induced by exosomal miR-320b. Notably, the miR-320b-PDCD4 axis activates the AKT pathway in HLECs independent of vascular endothelial growth factor-C (VEGF-C). Moreover, overexpression of miR-320b promotes the proliferation, migration, invasion, and epithelial-mesenchymal transition progression of ESCC cells. Finally, we demonstrate that METTL3 could interact with DGCR8 protein and positively modulate pri-miR-320b maturation process in an N6-methyladenosine (m6A)-dependent manner. Therefore, our findings uncover a VEGF-C-independent mechanism of exosomal and intracellular miR-320b-mediated LN metastasis and identify miR-320b as a novel predictive marker and therapeutic target for LN metastasis in ESCC.

INTRODUCTION

Esophageal cancer (EC) is the eighth most common cancer with the sixth highest mortality rate worldwide.[1,2] Among the two major histological subtypes of EC, esophageal squamous cell carcinoma (ESCC) accounts for about 80% of all EC cases.[3] Among the various clinical risk factors correlated with ESCC pathogenesis, lymph node (LN) metastasis remains the most important factor for poor outcomes, with 5-year postoperative survival rates in these patients decreasing from 70% to 18%.[1] ESCC patients with LN metastasis often present with a more malignant disease course with a higher probability for local and distant relapse, leading to a poor outcomes.[4] Despite the abundant evidence for the role of LN metastasis in cancer, the underlying molecular mechanisms that enhance it in ESCC remain unclear.

Lymphangiogenesis is an important process of generating new lymphatic vessels and is involved in LN metastasis in multiple tumors.[5–7] Growing evidence shows that lymphatic vessels in the tumor margin act as a channel for tumor cells to transmit from their local site to regional LNs.[8] However, the molecular mechanism of tumor-driven peritumoral lymphangiogenesis is not well defined. Among multiple factors underlying lymphatic metastasis, the adaptation of the primary tumor microenvironment by tumor cells to promote metastasis plays a crucial prometastatic role.[9] Previous studies suggested that tumor cells secreting VEGF-C is a critical step in ESCC lymphangiogenesis and LN metastasis.[10,11] However, about 21% of ESCC patients with LN metastasis show low VEGF-C expression,[12] which implies the existence of a VEGF-C-independent mechanism for lymphangiogenesis and LN metastasis in ESCC.

MicroRNAs (miRNAs) are small non-coding RNAs (18–26 nt) that target 3′ untranslated regions (3′ UTRs) of mRNAs, leading to the destabilization and/or posttranscriptional suppression.[13] Studies show that dysregulation of various miRNAs is closely related to tumorigenesis, progression, and recurrence.[14] Recent reports have

Received 6 June 2021; accepted 21 September 2021;
https://doi.org/10.1016/j.omto.2021.09.003.

[5]These authors contributed equally

Correspondence: Lutao Du, Department of Clinical Laboratory, The Second Hospital, Cheeloo College of Medicine, Shandong University, Jinan, Shandong 250033, China.
E-mail: lutaodu@sdu.edu.cn
Correspondence: Chuanxin Wang, Department of Clinical Laboratory, The Second Hospital, Cheeloo College of Medicine, Shandong University, Jinan, Shandong 250033, China.
E-mail: cxwang@sdu.edu.cn

suggested that miR-485-5p inhibits EC proliferation and invasion by downregulating the expression of O-GlcNAc transferase enzyme.[15] Moreover, miR-134 could modulate the proliferation, apoptosis, and LN metastasis of ESCC via the PLXNA1-mediated MAPK signaling pathway.[16] In addition, miR-10b-3p is considered an oncogene and a significant prognosis predictor in EC and can promote proliferation, migration, and invasion of ESCC through targeting FOXO3.[17] Nevertheless, the accurate expression and function of miRNA in ESCC LN metastasis progression has yet to be explored.

Despite previously considered to localize only in cells, miRNAs are now reported to be present extracellularly as a major RNA component in exosomes.[18] Exosomes are small microvesicles ranging from 30 to 150 nm in size that contain various types of nucleic acids, including miRNAs.[19,20] Recently, cancer-cell-released exosomes were identified as crucial mediators in cell-cell communication, which correlated with tumor-cell-induced vascular permeability,[21] premetastatic niche formation,[22] and bone marrow progenitor cell recruitment in distant organs.[23] However, the mechanism of cancer-cell-secreted exosome regulation of lymphatic vascular system formation via the induction of lymphangiogenesis remains unknown, warranting further exploration.

In this study, we report that a miRNA, miR-320b, was highly enriched in serum exosomes from patients with ESCC and correlated positively with LN metastasis. Exosomal miR-320b promoted lymphangiogenesis and LN metastasis *in vitro* and *in vivo*. Mechanistically, miR-320b was loaded to exosomes and transmitted to human lymphatic endothelial cells (HLECs). Subsequently, miR-320b suppressed programmed cell death 4 (PDCD4) expression and stimulated the AKT signaling pathway, facilitating lymphangiogenesis and LN metastasis in ESCC. Elevated expression of intracellular miR-320b could promote tumor cell proliferation, migration, and invasion through the miR-320b-PDCD4-AKT regulation axis. Our findings highlight a VEGF-C independent mechanism of exosomal and intracellular miR-320b-mediated LN metastasis and identify miR-320b as a potential predictive marker and therapeutic target for LN metastasis in ESCC.

RESULTS

Upregulation of serum exosomal miR-320b positively correlates with ESCC LN metastasis

To identify candidate exosomal miRNAs that play key roles in LN metastasis of ESCC, we first performed genome-wide miRNA next generation sequencing (NGS)-based miRNA expression profiling for 20 serum exosomes of ESCC patients (10 LN^-, 5 N1 stage, and 5 N3 stage cases). As shown in Figure 1A, overlapping differentially expressed miRNA (LN^- versus LN^+) analysis with differentially expressed miRNA (N1 stage versus N3 stage) analysis, we identified 11 exosomal miRNAs associated with LN metastasis. Subsequently, we excluded the low expression levels of miRNAs (average expression level < 50), which led to the selection of 3 miRNAs (miR-532-5p, miR-652-3p, and miR-320b). The three candidate miRNAs chosen by NGS were first investigated in clinical serum exosome samples consisting of 32 LN^- and 32 LN^+ ESCC patients. Results indicated that only exosomal miR-320b was highly expressed in the LN^+ group (2.555, 1.104–6.394) compared with the LN^- group (0.866, 0.293–2.122; $p < 0.001$, Figures S1A–S1C). An additional 114 clinical serum exosomal samples from ESCC patients (63 LN^- and 51 LN^+) were then analyzed with qRT-PCR, to validate the above phenomena. Thus, the training cohort comprised 95 LN^- and 83 LN^+ patients (cohort 1). In the training set, miR-320b was upregulated in LN^+ patients (3.129, 1.119–6.364) compared with LN^- patients (1.117, 0.493–2.346; $p < 0.001$, Figure 1B). The expression level of miR-320b in patients with N2–3 stage (5.505, 2.682–9.854) was also higher than in patients with N1 stage (2.16, 0.93–4.666; $p = 0.002$, Figure 1C). Receiver operating characteristic (ROC) curve analyses showed that miR-320b has a strong capability for discriminating LN^+ patients from LN^- patients and distinguishing N1 and N2–3 stage patients with an area under ROC curve (AUC) value of 0.737 (Figure 1D) and 0.707 (Figure 1E) in cohort 1, respectively. The expression level of miR-320b was further confirmed using another independent validation cohort (cohort 2) with 91 LN^- and 97 LN^+ patients. The alterations in the miR-320b expression pattern of the validation cohort agreed with those from the training cohort, with high expression in LN^+ (2.713, 1.179–5.523) compared with LN^- (1.301, 0.483–2.346; $p < 0.001$,) and N2–3 stage (4.17, 2.289–7.34) compared with N1 stage (2.233, 0.906–4.169; $p < 0.001$; Figures 1F and 1G). In compliance with the training cohort, the AUC of the cohort 2 was 0.715 and 0.715 (Figures 1H and 1I). Correspondingly, higher exosomal miR-320b levels strongly correlated incrementally with the peritumoral lymphatic vessel density (PLVD) in serial sections of ESCC specimens, as indicated by LYVE1-positive vessels using immunohistochemistry (IHC) analysis (Figure 1J). Correspondingly, Spearman's correlation analysis indicated that higher miR-320b levels strongly correlated with the increment of PLVD in serial sections of ESCC specimens ($r = 0.383$, $p = 0.002$, Figure 1K).

miR-320b containing exosomes are enriched in ESCC cell-secreted exosomes

Extracellular miRNAs have essential biological functions such as mediating cell-cell interactions and contributing to tumor LN metastasis. As they are mainly enriched in exosomes in particular,[24] we then examined miR-320b expression within ESCC-secreted exosomes. Exosomes purified from KYSE150 and EC9706 culture supernatant were detectable by transmission electron microscopy (TEM) and exhibited typical cup-shaped, round morphologies and were between 30 and 150 nm in diameter (Figure 2A). ZetaView analysis showed that the majority of the serum exosomes were 123.7 nm in diameter (Figure 2B). Increased exosome markers CD63 and CD9 protein and decreased levels of β-tubulin were observed compared with whole cells (Figure 2C). Notably, miR-320b was found to be enriched in ESCC-secreted exosomes, in particular, the EC9706 cell line (Figure 2D), relative to other cellular content and compared with exosomes secreted by non-carcinoma epithelial cell line (HET-1A).

To investigate the generation of secreted exosomal miR-320b by ESCC, we transfected a lentiviral vector overexpressing miR-320b or

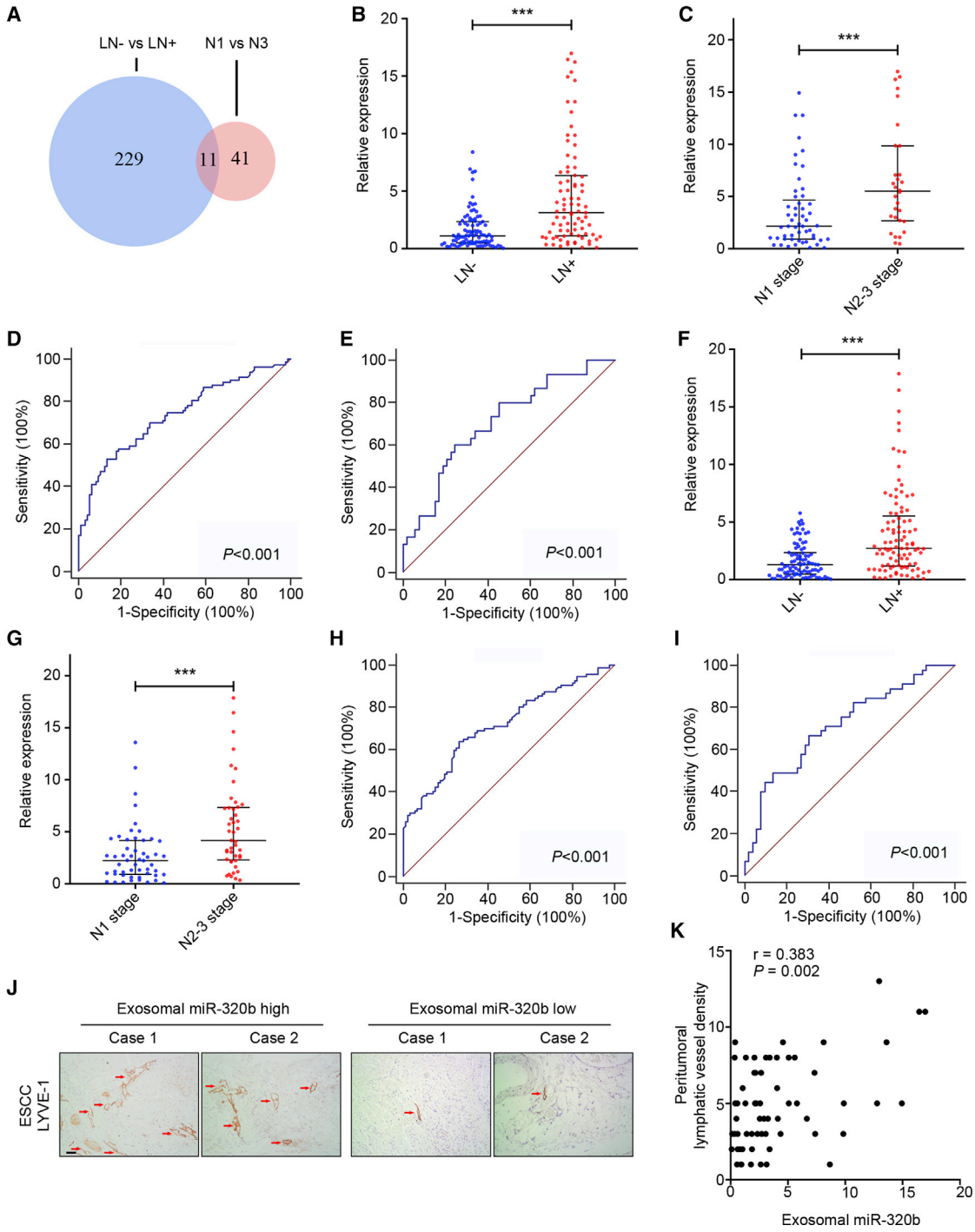

Figure 1. Exosomal miR-320b is associated with ESCC lymphatic metastasis

(A) Schematic of LN^- versus LN^+ and N1 versus N3 by NGS analysis for the identification of LN metastasis associated miRNAs. (B and F) qRT-PCR analysis of exosomal miR-320b in serum samples of ESCC patients in two cohorts. (C and G) qRT-PCR analysis of exosomal miR-320b in serum samples of LN^+ patients in two cohorts. (D and H) ROC curves for detection of LN metastasis using exosomal miR-320b as assessed by AUC in two cohorts. (E and I) ROC curve analysis of exosomal miR-320b for the discrimination of N stage in ESCC patients in two cohorts. (J) Staining of LYVE-1 protein in ESCC tissue specimens. The lymphatic vessels are indicated by red arrows. Scale bar, 50 μm. (K) Spearman's correlation analysis between serum exosomal miR-320b expression level and peritumoral lymphatic vessel density (PLVD) in ESCC tissues. ***$p < 0.001$.

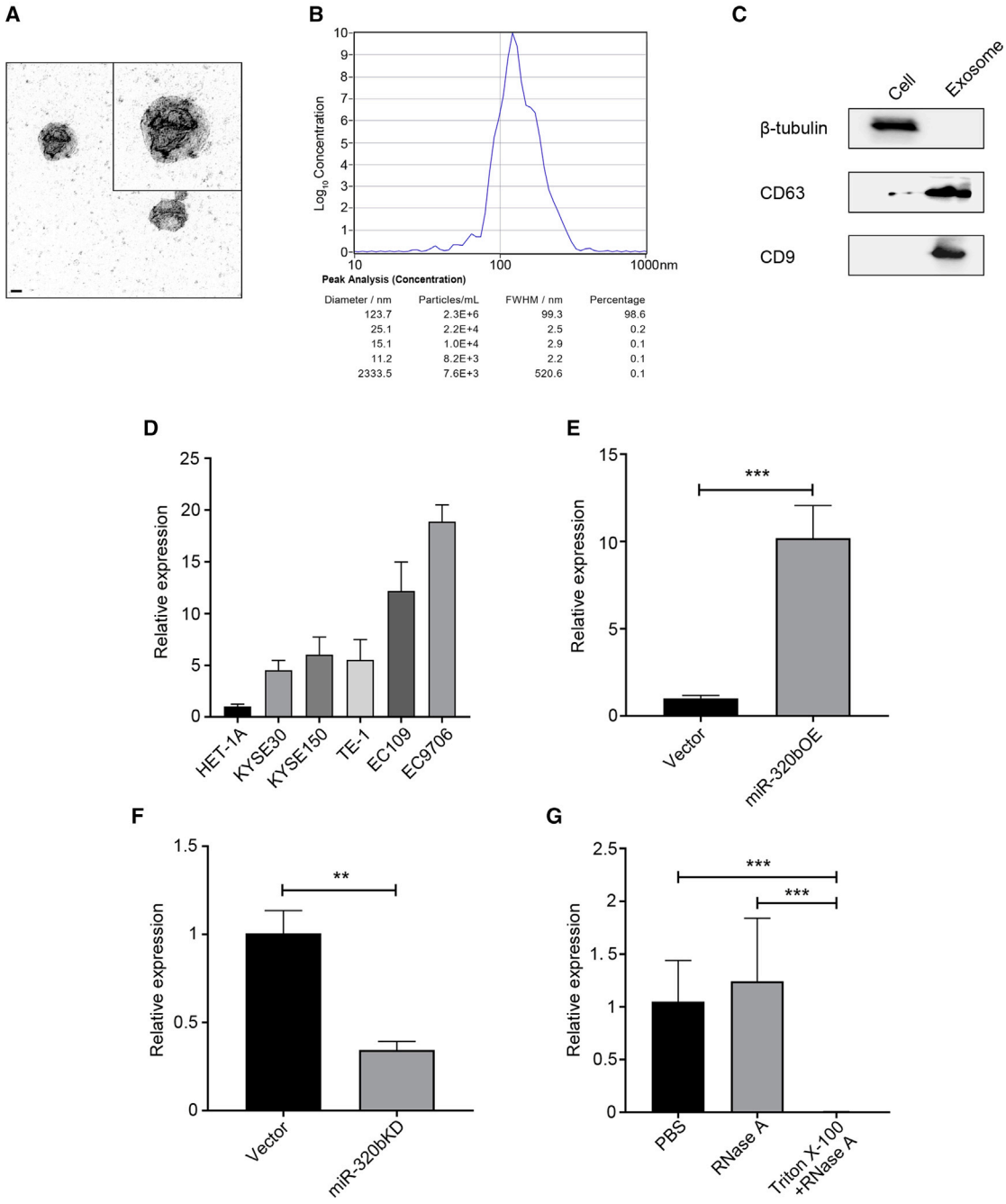

Figure 2. miR-320b is upregulated in ESCC cell-secreted exosomes

Isolated exosomes were confirmed by TEM (A) and Zetaview analysis (B). Scale bar, 50 nm. (C) Western blot analysis of CD9, CD63, and β-tubulin in lysates of exosomes or cells. (D) qRT-PCR analysis of miR-320b expression in exosomes from KYSE30, KYSE150, TE-1, EC109, EC9706, and HET-1A cells. miR-16 was used as an internal control. (E) qRT-PCR analysis of miR-320b expression in miR-320b overexpressing and control KYSE150 cells released exosomes. (F) qRT-PCR detection of miR-320b expression in miR-320b knocking down and control EC9706 cells released exosomes. (G) qRT-PCR analysis of miR-320b in the EC9706 cell-derived exosomes by treatment with PBS, RNase A (10 μg/mL), and/or 0.3% Triton X-100. ***$p < 0.001$.

scramble vector into KYSE150 (low miR-320b expressor). Conversely, lentiviral vector miR-320b knockdown or negative control (NC) was transfected into EC9706 (high miR-320b expressor). qRT-PCR analysis revealed that miR-320b expression was significantly higher in KYSE150-secreted exosomes ($KYSE150\text{-}EXO_{miR\text{-}320b}$) transfected with miR-320b overexpressing vectors and in NC EC9706-secreted

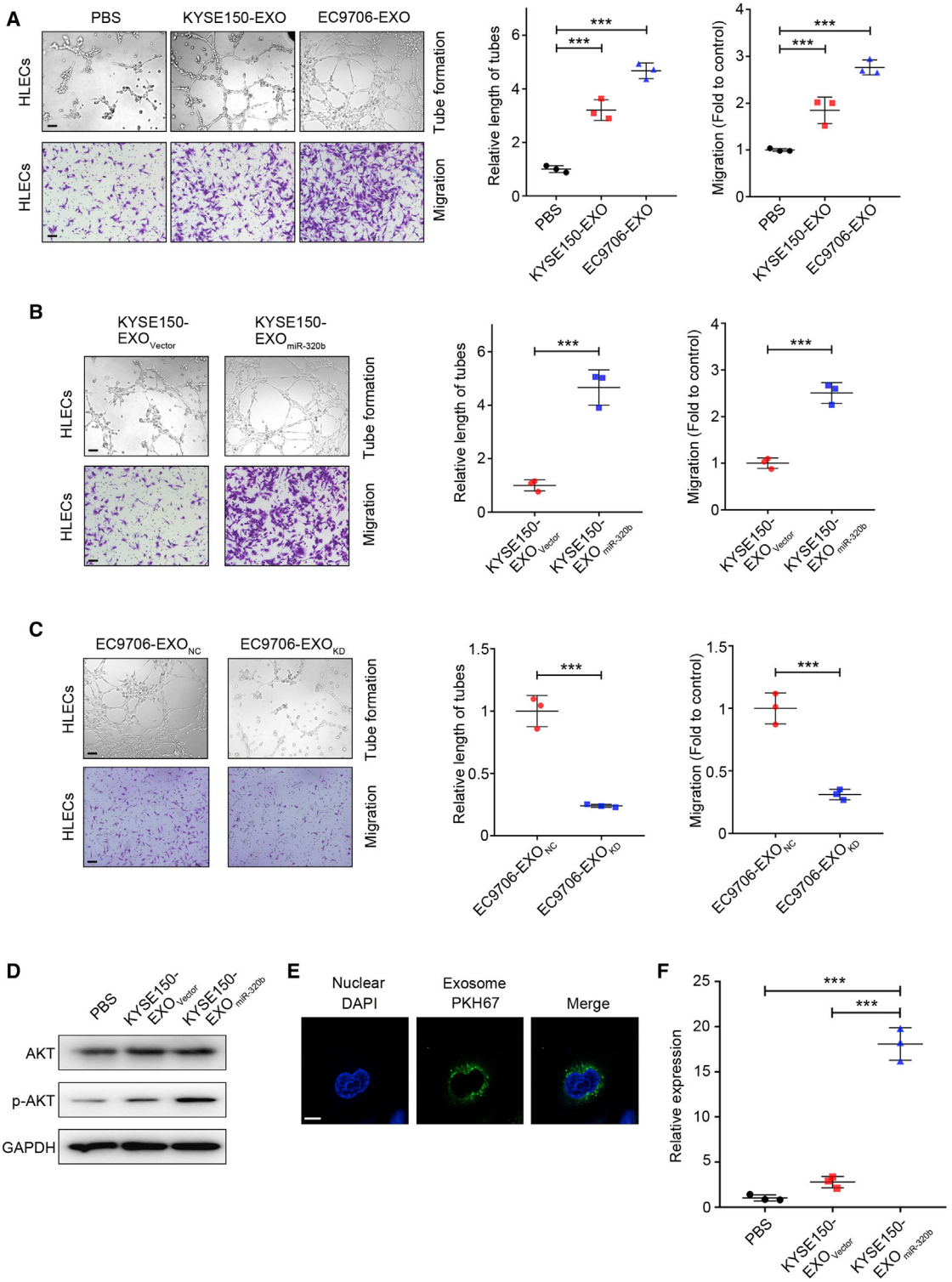

Figure 3. Exosomal miR-320b promotes lymphangiogenesis *in vitro*

(A) Representative images and quantification of tube formation and Transwell migration by HLECs treated with PBS, KYSE150-EXO, or EC9706-EXO. Scale bars, 100 μm. (B) Representative images and quantification of tube formation and Transwell migration by HLECs after treating with KYSE150-EXO$_{Vector}$ or KYSE150-EXO$_{miR\text{-}320b}$. Scale bars,

(legend continued on next page)

exosomes (EC9706-EXO_{NC}) than in scramble vector-transfected KYSE150 exosome (KYSE150-EXO_{Vector}) and that miR-320b knockdown EC9706 released exosomes (EC9706-EXO_{KD}; Figures 2E and 2F). To confirm that miR-320b was encapsulated within the lipid bilayer of exosomes and not directly released, we found miR-320b expression in culture medium unchanged upon RNase A treatment but significantly decreased with simultaneous treatment of RNase A and Triton X-100 together (Figure 2G).

Internalization of exosomal miR-320b by HLECs induces lymphangiogenesis

Since lymphangiogenesis is the rate-determining step for LN metastasis in ESCC,[25] we investigated whether miR-320b upregulation could facilitate lymphangiogenesis *in vitro*. We thus analyzed the effect of ESCC cell-secreted exosomes on HLEC tube formation and migration. We found that co-incubation with ESCC-secreted exosomes dramatically increased HLEC tube formation and migration compared with PBS (Figure 3A). Moreover, the KYSE150-$EXO_{miR\text{-}320b}$-derived exosome group had a higher HLEC tube formation and migration rate than the KYSE-EXO_{Vector} group (Figure 3B). Conversely, EC9706-EXO_{KD} co-incubation attenuated HLEC tube formation and migration rate (Figure 3C). As there is increasing evidence that suggests that AKT pathways are involved in lymphangiogenesis and lymphatic metastasis,[26] we were prompted to determine whether AKT signaling pathways in HELCs cells could be activated by exosomal miR-320b. We found that the phosphorylation levels of AKT significantly increased in HLECs with KYSE150-$EXO_{miR\text{-}320b}$ compared with KYSE150-EXO_{Vector} and PBS treatment groups (Figure 3D). These results indicate that exosomal miR-320b contributes to lymphangiogenesis *in vitro*.

Previous studies have demonstrated the ability of intracellular delivery of exosomal miRNAs.[27] Therefore, we investigated whether communication between ESCC cells and HLECs cells was possible via miR-320b-containing exosomes. We fluorescently labeled purified exosomes with membrane tracer PKH67 (green) and incubated them with HLECs cells. After 24 h of incubation, exosome co-cultured cells were stained with 4′,6-diamidino-2-phenylindole (DAPI, blue) for confocal microscopy evaluation. Detection of localized green-fluorescent signal within the cytoplasm of recipient HLECs indicated exosome internalization (Figure 3E). To confirm that miR-320b is successfully transferred to HLECs via exosomes, we measured miR-320b levels in HLECs pretreated with ESCC-secreted exosomes. A significantly higher level of intracellular miR-320b was observed in recipient HLECs following treatment with KYSE150-$EXO_{miR\text{-}320b}$ compared with PBS and KYSE-EXO_{Vector} treatments (Figure 3F). Moreover, prolonged incubation resulted in a corresponding increase in miR-320b levels in HLECs cells (Figure S1D). Additionally, actinomycin D (RNA polymerase II inhibitor) did not significantly alter miR-320b levels, excluding the possibility of endogenous induction of miR-320b in recipient cells (Figure S1E). Taken together, these results suggest that horizontal transfer of miR-320b from ESCC cells to HLECs can be performed intercellularly via exosomes.

ESCC-secreted exosomal miR-320b promotes LN metastasis *in vivo*

The effect of exosomal miR-320b on ESCC lymphangiogenesis and lymphatic metastasis was assessed *in vivo* using a popliteal LN metastasis model. We first randomly established footpad xenografts using luciferase-labeled KYSE150 cells, followed by intratumoral injection with PBS, KYSE150-EXO_{Vector}, or KYSE150-$EXO_{miR\text{-}320b}$ every 3 days. After eight injections, when primary tumor growth reached around 200 mm^3, mice were sacrificed, and the tumors and the associated popliteal LNs were harvested for IHC analysis (Figure 4A). Interestingly, IVIS® revealed that KYSE150-$EXO_{miR\text{-}320b}$ significantly promoted KYSE150 metastasis to the LNs compared with the PBS or KYSE150-EXO_{Vector}-injected groups (Figure 4B). The volume of popliteal LNs in the KYSE150-$EXO_{miR\text{-}320b}$-injected group was significantly larger than that in the control or KYSE150-EXO_{Vector} groups (Figures 4C–4E). Luciferase immunostaining indicated an increased number of metastatic LNs in the KYSE150-$EXO_{miR\text{-}320b}$ group, which confirmed that exosomal miR-320b significantly enhanced the metastatic potential of KYSE150 cells (Figures 4F and 4G). Moreover, the KYSE150-$EXO_{miR\text{-}320b}$-injected group exhibited significantly higher lymphangiogenic responses relative to the KYSE150-EXO_{Vector} group, resulting in shorter survival times (Figures 4H and 4I). Taken together, these results revealed that exosomal miR-320b plays an integral part in LN ESCC metastasis *in vivo*.

ESCC-secreted exosomal miR-320b targets PDCD4 to induce lymphangiogenesis

Multiple algorithms (TargetScan and miRanda) were used to identify the candidate targets of miR-320b, from which several target genes were predicted to be regulated by miR-320b. Among these candidates, PDCD4 expression, which could suppress the AKT signaling pathway, was significantly associated with LN metastasis and was chosen for further study (Figure 5A).[28–30] Dual-luciferase reporter assay in 293T cells indicated a significant and dose-dependent weakening in reporter activity for vectors containing the PDCD4 3′ UTR compared with control in the presence of miR-320b mimics (Figure 5B). When the miR-320b binding sites in the 3′ UTR were mutated, the reporter gene silencing was abrogated (Figure 5C), indicating that these are true miR-320b targeting sites. Consistent with the luciferase reporter assay results, treatment with KYSE150-$EXO_{miR\text{-}320b}$ but not the KYSE150-EXO_{Vector} and PBS resulted in a significant decrease of PDCD4 expression in HLECs at both RNA

100 μm. (C) Representative images and quantification of tube formation and Transwell migration by HLECs treated with EC9706-EXO_{NC} or EC9706-EXO_{KD}. Scale bars, 100 μm. (D) Western blot analysis of AKT pathway in HLECs treated with PBS, KYSE150-EXO_{Vector}, or KYSE150-$EXO_{miR\text{-}320b}$. (E) Labeled exosome (green fluorescent dye, PKH67) were taken up by HLECs cells (DAPI-labeled). Scale bar, 10 μm. (F) qRT-PCR analysis of miR-320b expression in HLECs treated with PBS, KYSE150-EXO_{Vector}, and KYSE150-$EXO_{miR\text{-}320b}$. ***$p < 0.001$.

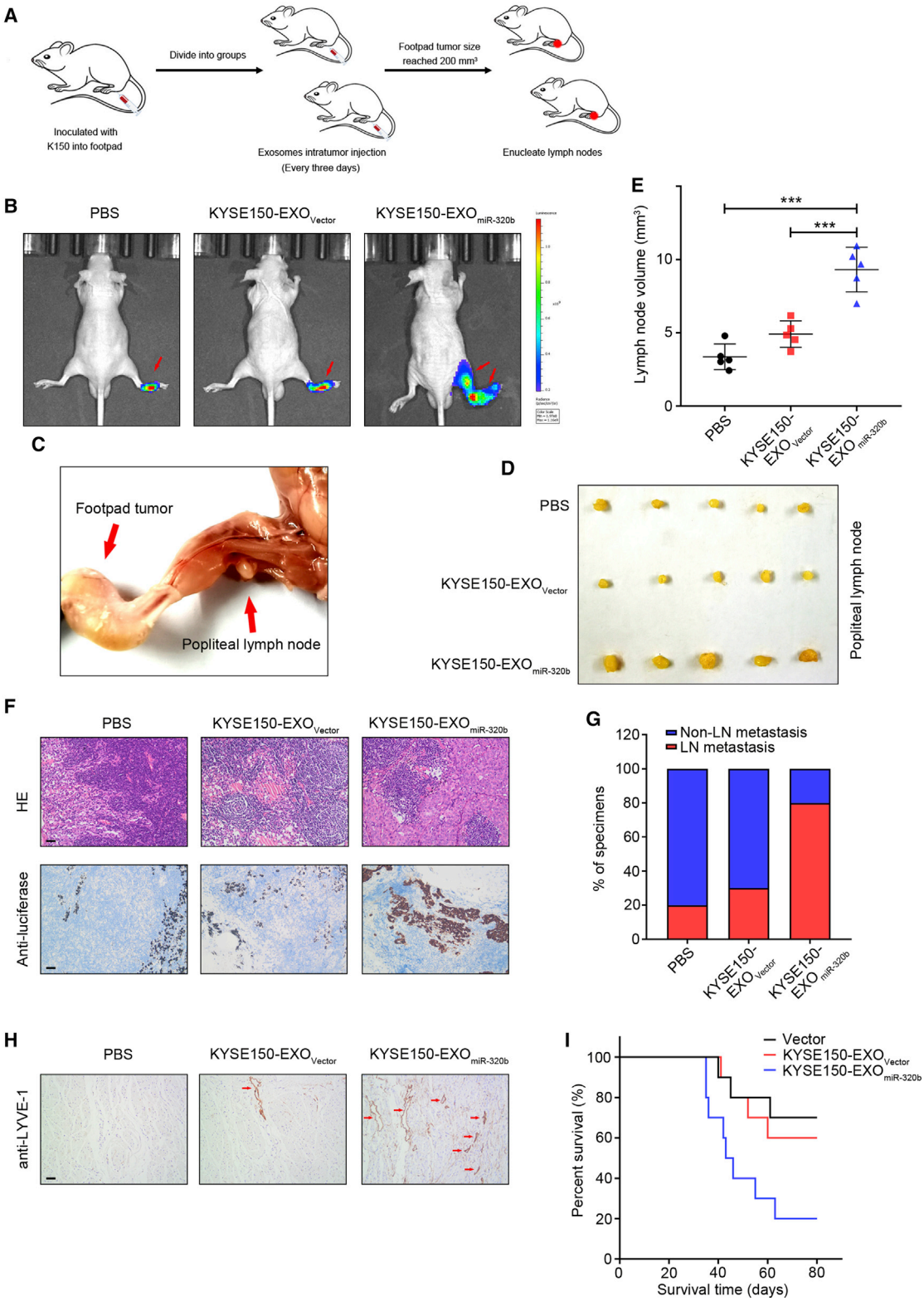

(legend on next page)

and protein levels (Figures 5D and 5E). Further *in vitro* studies confirmed that re-expression of PDCD4 rescued the downregulation of PDCD4 mediated by exosomes with high levels of miR-320b (Figure 5F). Further *in vitro* studies confirmed that re-expression of PDCD4 could rescue the downregulation of PDCD4 and upregulation of phosphorylated AKT level mediated by exosomes with high levels of miR-320b (Figure 5F). Most importantly, re-expression of PDCD4 abrogated KYSE150-$EXO_{miR\text{-}320b}$-mediated enhanced HLECs tube formation and migration (Figures 5G and 5H). Collectively, these results indicate that exosomal miR-320b induced lymphangiogenesis via suppression of PDCD4 expression in HLECs.

As a classic lymphangiogenic growth factor, tumor-derived VEGF-C could also induce lymphangiogenesis via activation of the AKT signaling pathways in HLECs,[31] and the relationship between miR-320b and VEGF-C expression was further examined in ESCC. Interestingly, VEGF-C-ELISA assay showed that miR-320b overexpression in KYSE150 or miR-320b knockdown in EC9706 did not alter the level of secreted VEGF-C (Figure 5I). Therefore, we concluded that the miR-320b-PDCD4 axis activated AKT signaling pathway and lymphangiogenesis functions in a VEGF-C-independent manner in HLECs.

miR-320b overexpression is correlated with ESCC LN metastasis through promoting ESCC malignant phenotypes

Tumorigenicity is also a significant factor underlying LN metastasis[32] and is closely associated with LN metastasis in various solid tumors, such as lung cancer,[33] gastric cancer,[34] and ESCC.[35] To procure an overall expression profile of miR-320b in cancers, we analyzed miR-320b expression levels in several types of cancers from the The Cancer Genome Atlas (TCGA) dataset (https://cancergenome.nih.gov). Almost all cancer tissues analyzed, including EC, had higher miR-320b expression levels than normal controls (Figure 6A). To verify the effect of miR-320b on the prognosis of cancer patients, we performed survival curves on Kaplan-Meier plots. As shown in Figure 6B, higher expression of miR-320b shortened the EC survival time. Collectively, these data indicated that miR-320b overexpression in EC tissues is correlated with poor outcomes in patients. Meanwhile, miR-320b was significantly upregulated in ESCC cancer cells compared with HET-1A (Figure 6C). Above all, these results indicated that miR-320b might play a crucial role in ESCC progression.

Based on these data, we further explored the pro-tumorigenic effect of miR-320b in ESCC cells. miR-320b overexpression (miR-320bOE) and knockdown (miR-320bKD) cell lines were established, and qRT-PCR was used to confirm transfection efficiency (Figures S2A and S2B). We found the proliferation of miR-320bOE KYSE150 was significantly enhanced, and miR-320bKD EC9706 cells were markedly inhibited compared with control groups, as was determined by cell counting kit-8 (CCK-8), colony formation, and EdU (5-ethynyl-2'-deoxyuridine) assays (Figures 6D–6F; Figures S2C–S2E). In addition, Transwell and wound healing assays demonstrate that the migration and invasion ability of miR-320bOE, KYSE150, and NC EC9706 cell lines were significantly increased compared with vector KYSE150 and miR-320bKD EC9706 cell lines (Figures 6G and 6H; Figures S2F and S2G). Finally, immunoblot analysis of epithelial-mesenchymal transition (EMT) marker revealed that miR-320b upregulation reduced E-cadherin protein levels but dramatically enhanced vimentin expression, with the inverse being true in miR-320b knockdowns (Figure 6I; Figure S2H). These data revealed that upregulation of miR-320b promotes ESCC proliferation, migration, invasion, and EMT progression.

We next investigated the tumorigenic capacity of miR-320b *in vivo* using a subcutaneous xenograft model as previously described.[36] Mice were inoculated subcutaneously with KYSE150 cells and randomly separated into three groups. Each group received intratumoral PBS, KYSE150-EXO_{Vector}, or KYSE150-$EXO_{miR\text{-}320b}$ every 3 days for 5 consecutive weeks (Figure 7A). KYSE150-$EXO_{miR\text{-}320b}$ enhanced tumor growth compared with both the KYSE150-EXO_{Vector} and PBS group (Figure 7B). Tumors in the KYSE150-$EXO_{miR\text{-}320b}$ group were of greater size and weight (Figures 7C–7E) and had higher expression levels of proliferation marker Ki67 than the KYSE150-EXO_{Vector} and PBS groups (Figure 7F). More importantly, as shown in Figure 7G, upregulated serum exosomal miR-320b levels strongly correlated with the incremental increase of Ki67-positive cells in ESCC tissues.

miR-320b promotes EMT progression and induces malignant phenotypes via targeting PDCD4 in ESCC cells

Functional experiments were performed to identify intracellular mediators of miR-320b-driven LN metastasis. Previous reports attribute PDCD4 as a tumor repressor gene, downregulated or lost in various cancer cells and linked with tumor progression and poor outcomes.[37–41] In this study, we performed TCGA dataset analysis and reveal that PDCD4 mRNA was significantly downregulated in EC tumor tissues than adjacent normal tissues (Figure S3A). Moreover, qRT-PCR and immunoblot assay indicated that the PDCD4 mRNA and protein levels were downregulated in ESCC cells compared with HET-1A cells (Figures S3B and S3C). The above bioinformatic analysis results with TargetScan and miRanda and Dual-Luciferase reporter system have also revealed the 3′ UTR of PDCD4 contains

Figure 4. Exosomal miR-320b promotes lymphatic metastasis *in vivo*

(A) Schematic representation of the popliteal LN metastasis nude mice model establishment. (B) Representative bioluminescent images of popliteal metastatic LN from nude mice treated with PBS, KYSE150-EXO_{Vector}, or KYSE150-$EXO_{miR\text{-}320b}$ (n = 5). Red arrow indicates footpad tumor and metastatic popliteal LN. (C) Representative image of the popliteal LN metastasis model. Representative images of enucleated popliteal LNs (D) and histogram analysis (E) of the LN volume of all groups (n = 5). (F) Representative images of IHC staining with anti-luciferase antibody (n = 5). Scale bars, 50 μm. (G) Percentages of LN metastasis in all groups (n = 10). (H) Staining of LYVE-1 protein in xenograft model primary tumor tissues. The lymphatic vessels are indicated by red arrows. Scale bar, 50 μm. (I) Kaplan-Meier survival curve for PBS, KYSE150-EXO_{Vector}, or KYSE150-$EXO_{miR\text{-}320b}$ groups (n = 10). ***$p < 0.001$.

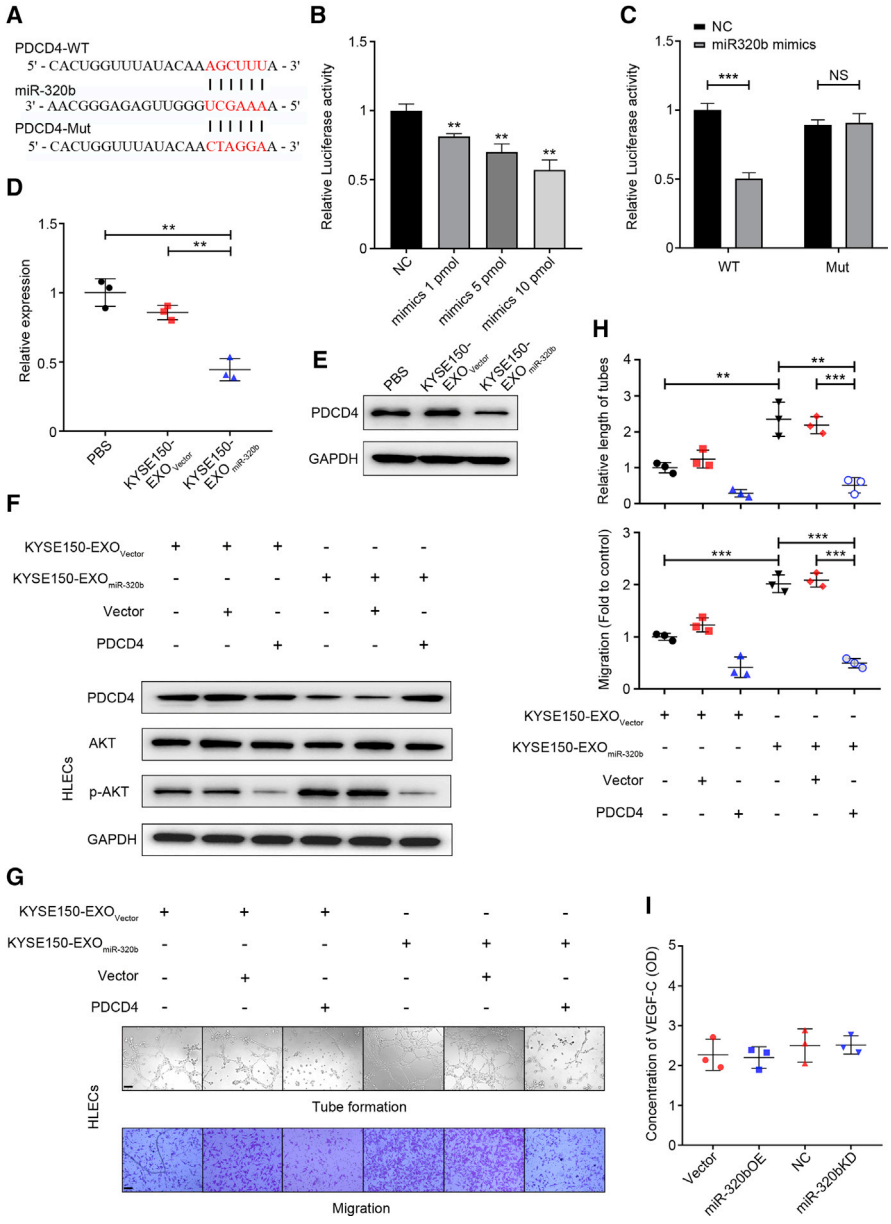

Figure 5. ESCC-secreted exosomal miR-320b targets PDCD4 to induce lymphangiogenesis

(A) Schematic representation of the putative predicted miR-320b targeting site in the PDCD4 mRNA 3′ UTR region. (B) Relative reporter gene activity of psiCHECK2 vector bearing PDCD4 3′ UTR fraction in 293T cells co-transfected with increasing amounts (1, 5, and 10 pmol) of miR-320b mimic. (C) Reporter gene activity of psiCHECK2 vector bearing PDCD4 3′ UTR wild-type (WT) fraction or their mutant type (Mut) fraction in 293T cells in the presence of 10 pmol miR-320b mimics. Treatment with PBS, KYSE150-EXO_{Vector}, or KYSE150-$EXO_{miR\text{-}320b}$ on the levels of PDCD4 RNA (D) and PDCD4 protein (E) in HLECs. (F) Protein levels of PDCD4 and AKT pathway were, respectively, detected by western blot in HLECs treated with indicated exosomes in the presence of PDCD4 overexpression plasmid or vector. Representative images (G) and histogram analysis (H) of tube formation and migration by HLECs treated with KYSE150-EXO_{Vector} or KYSE150-$EXO_{miR\text{-}320b}$ and then transfected with vector or PDCD4 plasmid. Scale bars, 100 μm. (I) ELISA assay shows the expression level of VEGF-C in the ESCC cells culture medium of different groups. $^{**}p < 0.01$, $^{***}p < 0.001$.

a binding site for miR-320b. In the present study, our data indicate PDCD4 mRNA and protein levels were lower in miR-320b overexpressing cells and higher in miR-320b knockdown cells compared to controls (Figures 8A and 8B; Figures S3D and S3E). *In vivo*, KYSE150-$EXO_{miR\text{-}320b}$ could significantly enhance the expression level of PDCD4 protein through IHC assay (Figure S3F). Furthermore, we found an inverse correlation between miR-320b and PDCD4 mRNA levels ($r = -0.412$, $p = 0.006$) in ESCC tissues

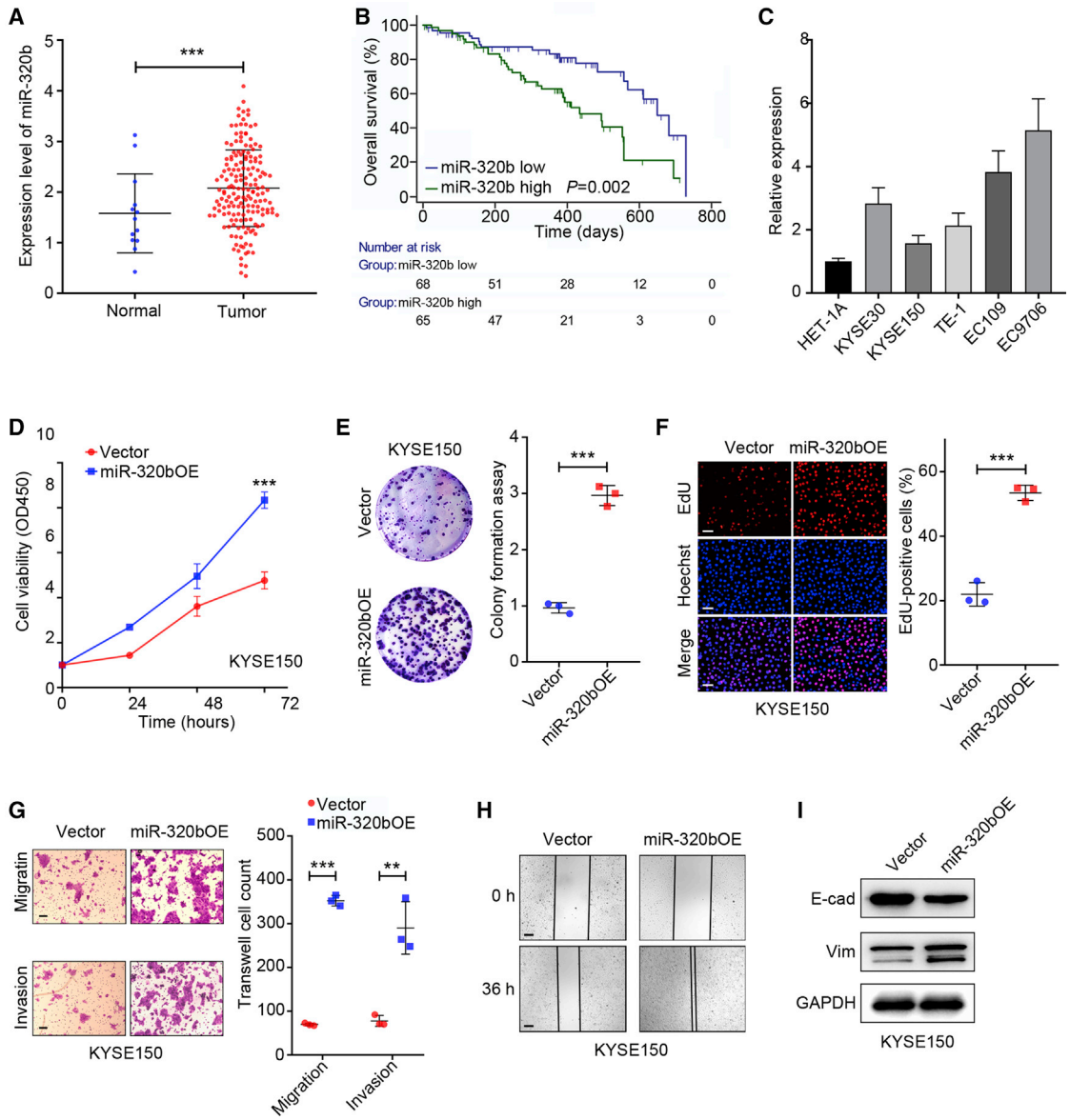

Figure 6. miR-320b overexpression is correlated with ESCC LN metastasis through promoting ESCC malignant phenotypes

(A) TCGA database analysis of miR-320b expression in EC and adjacent normal tissues. (B) Survival curves of EC patients with alteration miR-320b levels was calculated in Kaplan-Meier method. (C) qRT-PCR analysis to exanimate the miR-320b expression in KYSE30, KYSE150, TE-1, EC109, EC9706, and HET-1A cells. (D) Cell proliferation was examined by CCK-8 assay in KYSE150 cell with indicated treatment. (E) Colony formation assay of KYSE150 cells followed by indicated treatment. (F) EdU proliferation assay of KYSE150 cells followed by indicated treatment. Scale bars, 50 μm. (G) Migration and invasion ability of indicated treatment cells were assessed by Transwell assay. (H) Motility ability of indicated treatment cells were assessed by wound healing assays. Scale bars, 100 μm. (I) Western blot analysis of protein E-cadherin (E-cad) and Vimentin (Vim) expression in indicated treatment cells. ***p < 0.001.

(Figure 8C). Therefore, PDCD4 are likely functional targets of miR-320b in ESCC cells.

Since PDCD4 regulates AKT signaling, we next examined whether miR-320b affects AKT signaling through PDCD4 in ESCC cells. We found that knockdown of PDCD4 expression by small interfering RNA (siRNA) substantially activated signaling as indicated by increased AKT phosphorylation (Figure S3G). The inverse effect of miR-320b has on AKT signaling through alleviating PDCD4-mediated suppression was evident in cells with miR-320b knockdown or overexpression (Figure 8B). Next, rescue assays showed that knockdown of PDCD4 partially reversed the suppression of AKT signaling due to miR-320b knockdown in malignant phenotypes of ESCC cells (Figures 8D–8J; Figures S4A–S4G). These results

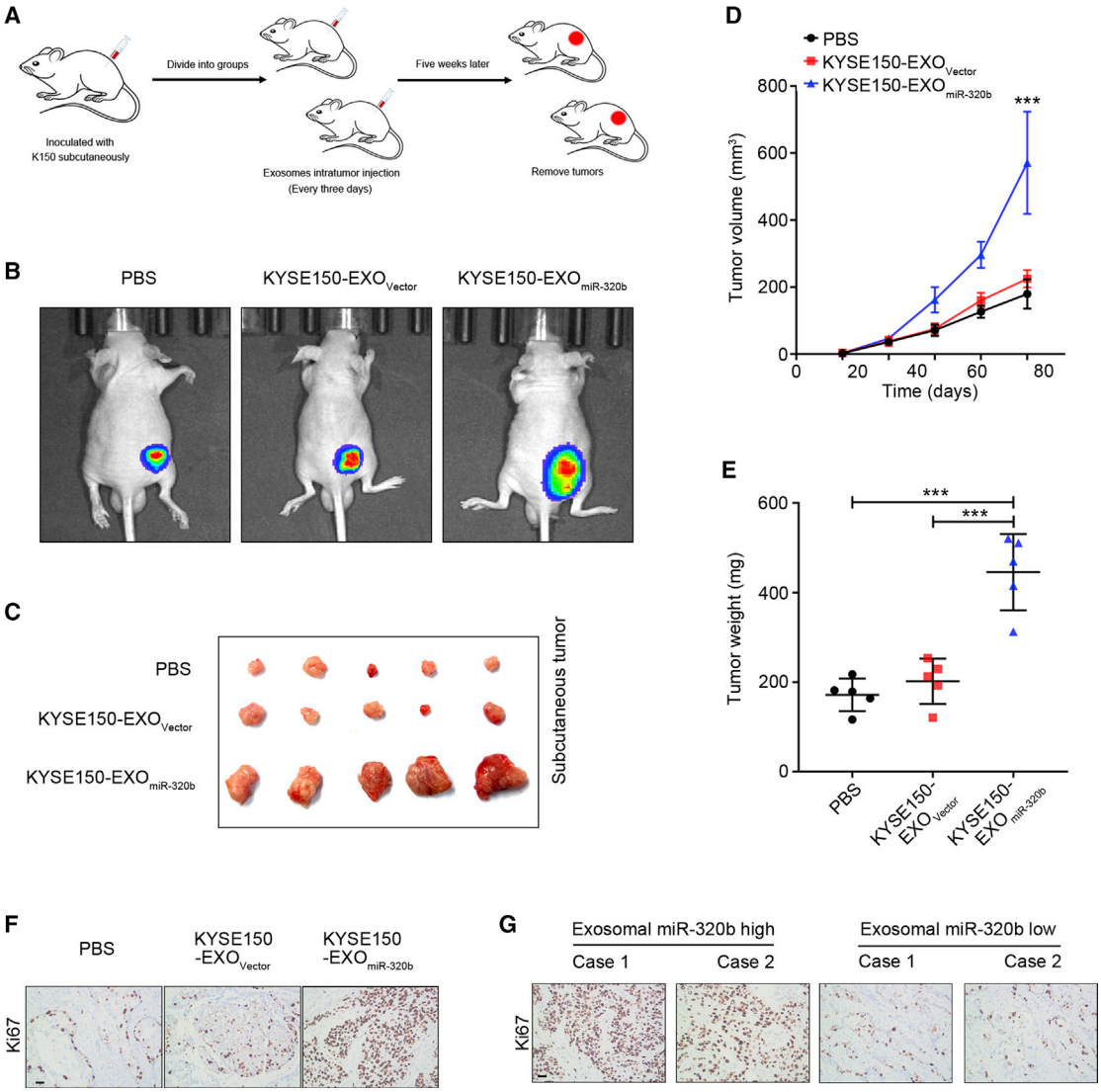

Figure 7. Exosomal miR-320b promotes ESCC tumorigenesis *in vivo*

(A) Schematic representation of the xenograft model establishment. (B) Representative bioluminescence images of subcutaneous tumors from nude mice treated with PBS, KYSE150-EXO$_{Vector}$, or KYSE-EXO$_{miR-320b}$ (n = 5). (C) Representative images of subcutaneous tumors from nude mice treated with PBS, KYSE150-EXO$_{Vector}$, or KYSE-EXO$_{miR-320b}$ (n = 5). Tumor volume (D) was measured every 5 days and weights (E) were measured after tumor resection (n = 5). (F) Representative images of IHC staining for Ki67 expression (n = 5) in xerograph model tumor tissues. (G) Representative images of IHC staining for Ki67 expression in clinical ESCC patients' tumor tissues. Scale bars, 50 μm. ***$p < 0.001$.

suggest that miR-320b acts as an upstream activator of AKT signaling and malignant phenotypes through inhibition of PDCD4 production in ESCC.

METTL3-dependent N6-methyladenosine (m6A) regulates the processing of miR-320b by DGCR8

Recently, Alarcon and colleagues[42] demonstrated that m6A modification by METTL3 marks pri-miRNAs for recognition and processing to mature miRNA by DGCR8, which suggests that altered METTL3/m6A might contribute to the aberrant expression of miRNAs in many biological processes, including cancers. It was also previously demonstrated that METTL3 was significantly upregulated in EC tissues, compared with the adjacent tissues, which was consistent with the results from tissue samples in TCGA database (Figure 9A). We further examined METTL3 protein expression in esophageal-associated cell lines. As shown in Figure S4H, METTL3 expression was significantly upregulated in ESCC cells as compared with that in human normal esophageal epithelial cells (HET-1A), especially in EC9706 cells. To verify the role of the METTL3-m6A modification in the pri-miR-320b processing, we

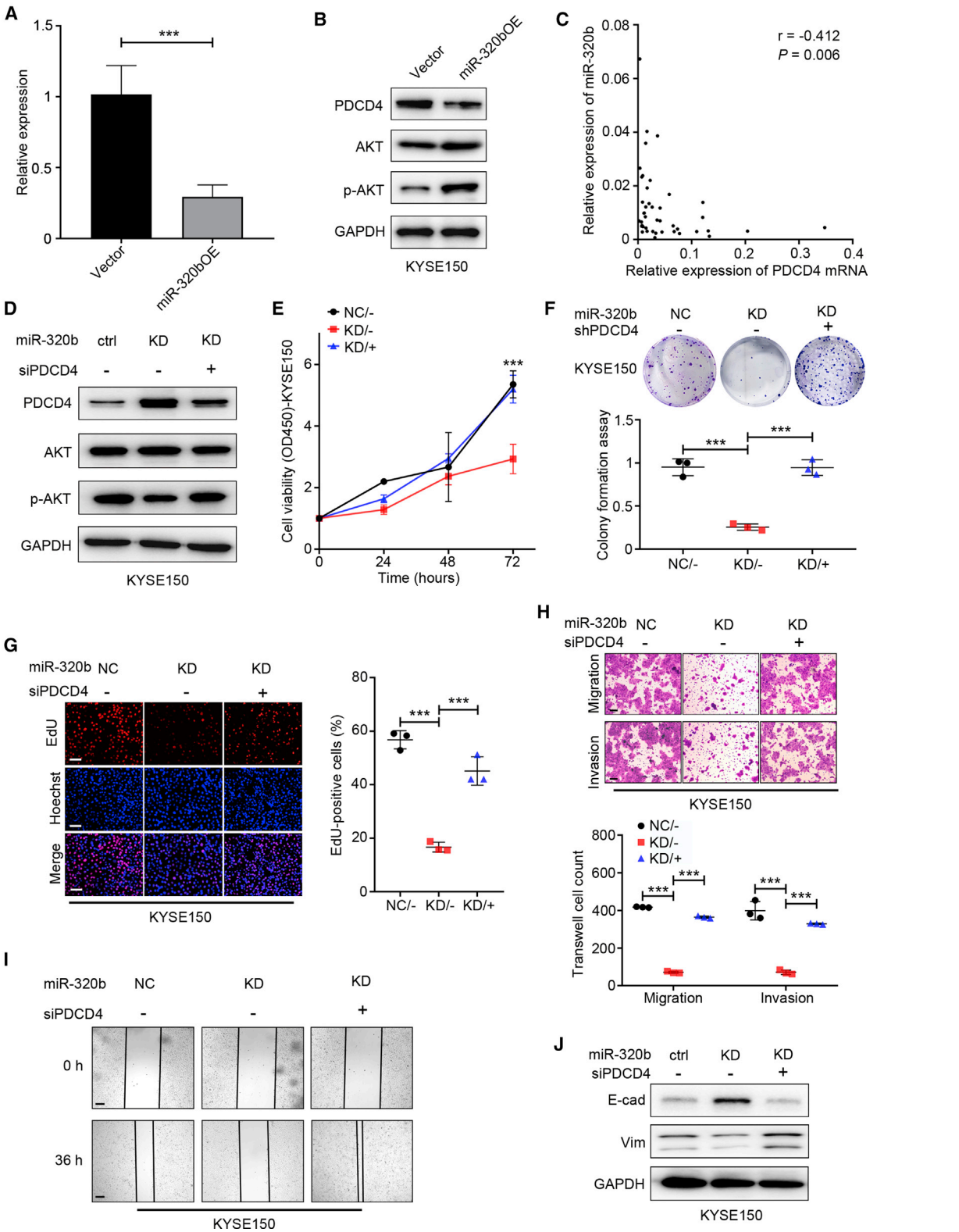

(legend on next page)

used SRAMP database (http://www.cuilab.cn/sramp) to identify two putative m6A sites (RRACH sequence motifs) located in pri-miR-320b. Consistently, a positive correlation between METTL3 mRNA and miR-320b levels was observed in tumor tissues from ESCC patients (Figure 9B).

Therefore, we hypothesized that METTL3 contributes to ESCC LN metastasis by targeting miR-320b in an m6A-dependent pri-miRNA-processing manner. To elucidate the mechanism of METTL3 in the production of mature miR-320b, we compared the expression levels of pri-miR-320b, pre-miR-320b, and miR-320b in METTL3-overexpressing or knockdown cell lines (Figure 9C). Consistent with our hypothesis, overexpression of METTL3 in cells significantly decreased pri-miR-320b levels but increased both pre-miR-320b and miR-320b levels, whereas knocking down METTL3 markedly reversed this trend (Figures 9D–9F).

We further assessed whether METTL3 was required for the engagement of pri-miR-320b by the microprocessor protein DGCR8. As shown in Figure 9G, immunoprecipitation assay revealed that METTL3 co-precipitates with DGCR8 and ribonuclease treatment could weaken their interaction, suggesting that their interaction might be partly mediated by RNAs. We next observed a significant increase in m6A methylated RNA bound by DGCR8 in METTL3-overexpressing cells (Figure 9H). These findings suggest that METTL3 could manipulate pri-miR-320b processing by regulating the recognition and binding of DGCR8 to pri-miR-320b. Further, we also observed increased levels of pri-miR-320b bound to DGCR8 by qRT-PCR in METTL3-overexpressing cells compared to control when we immunoprecipitated DGCR8 (Figure 9I). Moreover, when we immunoprecipitated m6A from RNAs of control and METTL3-overexpressing cells, we found that METTL3 overexpression significantly increased the amount of pri-miR-320b modified by m6A (Figure 9J). Together, these results indicate that the METTL3 could enhance the recognition of pri-miR-320b by DGCR8, leading to processing to mature miRNA in an m6A manner.

DISCUSSION

Herein, our study demonstrated that not only was miR-320b enriched in serum exosome profiles from patients with ESCC, but serum exosomal miR-320b were positively associated with lymphatic metastasis in these patients. Moreover, we identified that tumor-secreted exosomal miR-320b could be internalized by HLECs, which enhanced AKT phosphorylation through targeting PDCD4 mRNA 3′ UTR and alleviating PDCD4-mediated suppression, resulting in the lymphangiogenesis and lymphatic metastasis of ESCC in a VEGF-C-independent manner. Additionally, intracellular expression of miR-320b in ESCC promoted its proliferation, migration, and invasion. These findings provide an in-depth mechanistic and translational insight into the pathways by which exosomal and intracellular miRNA promotes ESCC lymphatic metastasis, while supporting the emergence of miR-320b as an LN metastatic prediction marker and novel therapeutic target in ESCC (Figure 9K).

The occurrence of regional LN metastasis at an early stage is considered a crucial step in ESCC progression.[4] Therefore, it is necessary to identify novel and effective biomarkers that discriminate between indolent and aggressive ESCC in developing personalized diagnostic and therapeutic strategies for patients with different progression risks. Our clinical data revealed that serum exosomal miR-320b was positively associated with PLVD and LN metastasis in patients with ESCC, suggesting that circulating exosomal miR-320b may serve as a potential early prediction biomarker for LN metastasis. Exosomes have been extensively studied for their function in intercellular communication between the tumor and the tumor microenvironment.[19] Recently, cancer-secreted exosomal miRNAs have emerged as highly versatile regulators within this communication process.[43] Zhou et al.[44] reported that uptake of cancer-secreted miR-105 by vascular endothelial cells provoked vascular permeability and metastatic dissemination. Our results showed that ESCC-secreted miR-320b could be horizontally transferred to HLECs to promote lymphangiogenesis and facilitate lymphatic metastasis, suggesting that miR-320b may represent a potential molecular target for clinical intervention in ESCC patients with LN metastasis.

Another important finding in the present study was that cancer-secreted exosomal miR-320b downregulated PDCD4 expression in HLECs. Previous studies suggest that PDCD4 can be a critical factor for angiogenesis by regulating various signaling pathways, including VEGF-STAT3, c-Jun, and AKT.[45–47] Importantly, overexpression of PDCD4 in abnormal vascularization of tumors could affect Ang-2 expression and release. Hence, the induction of PDCD4 may be a new therapeutic avenue to inhibit cancer metastasis by suppressing Ang-2.[48] Although several studies have indicated the essential role of PDCD4 in angiogenesis, cancer-induced PDCD4 transcription in HLECs remains unknown. Herein, we demonstrated that ESCC cell-secreted exosomal miR-320b downregulated PDCD4 expression in HLECs via the PDCD4 mRNA 3′ UTR binding site. PDCD4 overexpression abolished the lymphangiogenesis-stimulating effect induced by exosomal miR-320b. Therefore, our findings uncovered what we believe is a novel molecular mechanism underlying

Figure 8. miR-320b promotes ESCC progression by targeting PDCD4

qRT-PCR (A) and western blot (B) analysis of PDCD4 mRNA, protein, and AKT pathway in ESCC cells after stable overexpression of miR-320b. (C) Spearman's correlation analysis between PDCD4 mRNA levels and miR-320b levels in ESCC tissues (n = 43). (D) Western blot analysis of PDCD4 protein and AKT pathway expression in KYSE150 cells followed by indicated rescue experiment treatment. Cell proliferation was examined by CCK-8 (E), colony formation (F), and EdU (G) assay in KYSE150 cell with indicated rescue experiment treatment. (H) Migration and invasion ability of indicated rescue experiment treatment cells were assessed by Transwell assay. (I) Motility ability of indicated rescue experiment treatment cells were assessed by wound healing assays. Scale bars, 100 μm. (J) Western blot analysis of protein E-cadherin (E-cad) and Vimentin (Vim) expression in indicated rescue experiment treatment cells. ***$p < 0.001$.

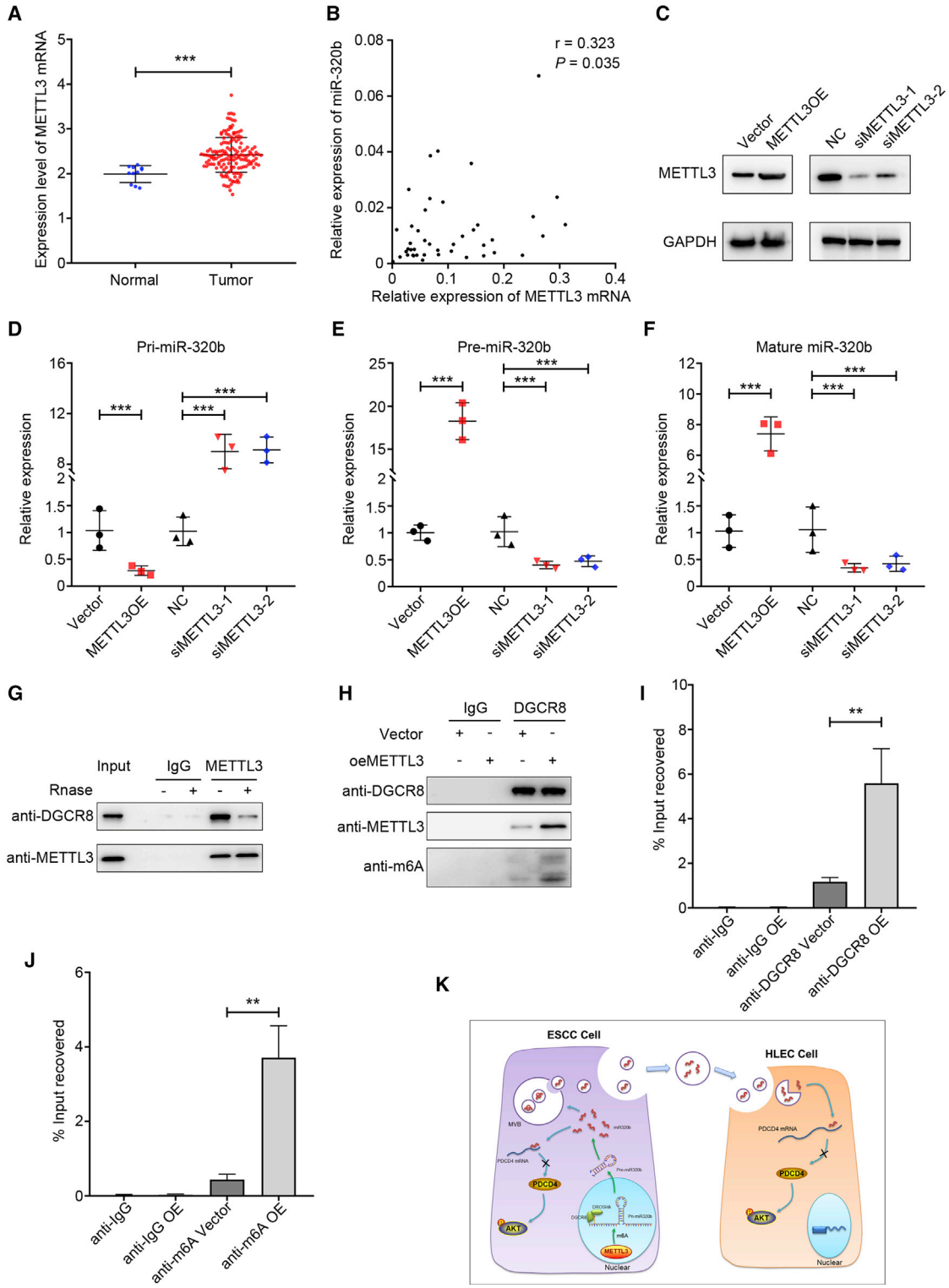

Figure 9. METTL3-dependent m6A methylation modulates the processing of miR-320b by DGCR8

(A) TCGA database analysis of METTL3 expression in ESCA. (B) Spearman's correlation analysis between METTL3 mRNA levels and miR-320b levels in ESCC tissues (n = 43). (C) Western blot analysis shows the expression level of METTL3 mRNA and protein in METTL3 overexpress and knockdown KYSE150 cell. (D–F) METTL3

(legend continued on next page)

cancer-secreted exosomal miRNA-mediated PDCD4 downregulation in HLECs, resulting in lymphangiogenesis and LN metastasis, thus expanding the current knowledge regarding PDCD4 regulation in HLECs. It is noteworthy that exosomal miR-320b engage in the transference of genetic information, whereas lymphangiogenic growth cytokines such as VEGF-C are small proteins. These represent two different yet potentially interactive methods for signal transmission between cancer cells and HLECs. Previous studies have demonstrated that VEGF-C signaling induced lymphangiogenesis via activation of AKT pathways.[24] Our study found that HLECs treated with exosomes with high miR-320b led to increased phosphorylation of AKT proteins, which presents a potential mechanism for intercellular miR-320b-PDCD4 axis induced lymphangiogenesis in ESCC. These results imply that the miR-320b-PDCD4 axis and VEGF-C might share the same downstream pathways for lymphangiogenesis. Therefore, we considered that the miR-320b-PDCD4 axis activated AKT signaling pathways and might work in a VEGF-C-independent manner in HLECs. Developing personalized therapeutics, such as VEGF-C-independent lymphangio-miR-320b that might serve as anti-LN metastasis targets in combination with current anti-VEGF-C therapies, might establish a new strategy for treating early-stage ESCC patients with LN metastasis.

We also found that miR-320b was overexpressed in EC tissues and related to the poor outcomes of cancer patients using the TCGA dataset analysis. Meanwhile, miR-320b was significantly upregulated in ESCC cancer cells compared with HET-1A. Moreover, upregulating miR-320b positively promoted the proliferation, migration, and invasive ability of ESCC cells, which demonstrated miR-320b might play an essential role in LN metastasis of ESCC. More importantly, our results also revealed that overexpressed miR-320b decreased the expression of PDCD4, increased expression of p-AKT, and induced EMT and metastatic ability in ESCC cells. PDCD4 downregulation in ESCC cells promoted the expression of p-AKT and induced EMT. Meanwhile, overexpression of PDCD4 in recipient ESCC cells significantly reversed the effects of miR-320b. Hence, it is possible that miR-320b activates EMT and promotes ESCC LN metastasis by directly targeting PDCD4.

As the main component in the so-called m6A "writer," METTL3 was reported to promote bladder cancer progression by an m6A-dependent manner.[49] In the present study, we found that METTL3 was upregulated in EC tissues and cells and could regulate the expression of pri-miR320b, pre-miR-320b, and miR-320b in ESCC cells. Moreover, METTL3 could interact with the microprocessor protein DGCR8 and positively modulate the pri-miR-320b process in an m6A-dependent manner. These imply that METTL3 could promote the maturation of pri-miR-320b in ESCC through m6A.

In conclusion, our data provided evidence that high levels of serum exosomal miR-320b are associated with LN metastasis and are positively correlated with PLVD in ESCC. Horizontal transfer of ESCC-secreted exosomal miR-320b into HLECs may promote lymphangiogenesis by regulating PDCD4 signaling, and intracellular miR-320b enhanced the malignant phenotypes of ESCC cells, which synergistically promotes LN metastasis. The newly identified vicious METTL3/m6A-miR-320b-PDCD4-AKT axis illustrates a critical molecular mechanism of ESCC progression and develops a potential noninvasive diagnostic approach and therapeutic strategy for ESCC patients with LN metastasis.

MATERIALS AND METHODS

Patient sample collection

A total of 366 patients underwent esophagectomy for the treatment of ESCC at the Department of General Surgery of Qilu Hospital, Cheeloo College of Medicine, Shandong University, and the Second Hospital, Cheeloo College of Medicine, Shandong University, between November 2017 and December 2020 were enrolled in this study. None of the patients had distant metastasis, underwent any prior chemo- or radiotherapy, or suffered from other co-current malignant disorders. Tumor stage was defined according to the classification guidelines of the American Joint Committee on Cancer (AJCC, 8th edition).[50] All clinical patient characteristics are listed in Supplementary Table S1. This study was approved by the Clinical Research Ethics Committee of The Second Hospital, Cheeloo College of Medicine, Shandong University, and informed consent was obtained from all participants.

Cell lines and culture

Human ESCC cell lines (KYSE30, KYSE150, TE-1, EC109, and EC9706) and immortalized esophageal epithelial cell line (HET-1A) was purchased from Type Culture Collection of the Chinese Academy of Sciences (Shanghai, China). KYSE30 and KYSE150 were cultured in RPMI 1640 medium (GIBCO) supplemented with 10% fetal bovine serum (FBS). TE-1, EC109, and EC9706 cell lines were cultured in DMEM (GIBCO) supplemented with 10% FBS. HLECs were purchased from ScienCell Research Laboratories and cultured in ECM complete medium (ScienCell Research Laboratories). For exosomes co-culture, 1 μg/mL (as determined by BCA protein assay (Thermo Fisher Scientific, USA) of exosomes were added to the culture medium of recipient cells (5×10^6).

In vivo

Luciferase-labeled KYSE150 cells (5×10^6) were inoculated into the footpads of BALB/c nude mice (4–5 weeks old, 18–20 g) to establish the popliteal lymphatic metastasis model. Mice were then randomly divided into three groups (n = 5 or 10 per group). PBS, KYSE150-EXO_{Vector}, or KYSE150-$EXO_{miR\text{-}320b}$ (5 μg/dose) was injected

overexpression or knockdown significantly affected the expression of pri-miR-320b, pre-miR-320b, and miR-320b in PDAC cells. (G) Coimmunoprecipitation of the METTL3-interacting protein DGCR8. (H) Immunoprecipitation of DGCR8, METTL3, and m6A associated RNA from control cells or cells overexpressing METTL3. (I) Immunoprecipitation of DGCR8-binding pri-miR-320b from control or METTL3-overexpressing cells followed by qRT-PCR analysis. (J) Immunoprecipitation of m6A-modified pri-miR-320b from control or METTL3-overexpressing cells followed by qRT-PCR analysis. (K) Proposed model of exosomal and intracellular miR-320b promotes lymphatic metastasis in esophageal squamous cell carcinoma. $^{**}p < 0.01$, $^{***}p < 0.001$.

intratumorally every 3 days. LN metastasis was analyzed using an *In Vivo* Imaging System (Spectrum CT, PerkinElmer, USA). Footpad tumors and popliteal LNs were resected when tumor growth reached 200 mm^3 (LN volume = 0.5 × $width^2$ × length). Pathological sections of primary tumors and popliteal LNs were analyzed by IHC and visualized on an inversion microscope (Zeiss, Germany). For survival analysis, mice were performed until death or 80 days after the first PBS or exosomes injection.

KYSE150 cells (5×10^6 cells per mouse) were injected subcutaneously into the right back of nude mice to establish the subcutaneous tumor growth assay. 14 days later, when tumor growth reached about 200 mm^3 in size, purified KYSE150-EXO_{Vector}, or KYSE150-$EXO_{miR\text{-}320b}$ (5 μg/dose) or PBS was injected intratumorally, and tumor size and body weight were measured twice weekly. Mice were sacrificed 7 weeks' post, and tumor tissues (tumor volume = 0.5 × $width^2$ × length) were prepared for histological examination. All animal work was performed according to the Health guidelines, and protocols were approved by the Institutional Animal Care and Use Committee of Shandong University.

Fluorescence assay

PKH67 (Sigma-Aldrich, USA; 1 μM) was used to label exosomes according to the manufacturer's instructions. PKH67-labeled exosomes were cocultured with HLECs for 24 h, followed by cell nuclear staining with DAPI (Invitrogen, USA). The HLECs cells were fluorescently visualized with a laser scanning microscope Axio-Imager-LSM800 (Zeiss, Germany).

Tube formation assay

Growth factor reduced Matrigel (BD Biosciences, CA, USA) was used to precoat 96-well plate and incubated at 37°C for 2 h, followed by tube formation of seeded 2×10^4 HLECs treated with either PBS or exosomes for 6 h. The tubes were visualized with an inverted microscope, and the length of lymphatic tubes was analyzed using ImageJ software.

RNA immunoprecipitation assay

RNA immunoprecipitation (RIP) assays were performed using the EZ-Magna RIP kit (Millipore). Lysates of 1×10^7 KYSE150 cells obtained using complete RIP lysis buffer were immunoprecipitated with RIP buffer containing anti-DGCR8 and anti-m6A antibody-conjugated dynabeads. Total RNA (input control) and isotype control (immunoglobulin G, IgG) for each antibody were assayed simultaneously. The co-precipitated pri-miR-320b were detected by qRT-PCR, which was normalized to input.

Bioinformatics analysis

The potential target mRNA of miR-320b was predicted using the TargetScan database (http://www.targetscan.org/) and http://www.microrna.org/ miRanda software. The m6A binding motifs of pri-miR-320b was predicted by SRAMP (http://www.cuilab.cn/sramp).

Data availability

The NGS data for this study are available on the Gene Expression Omnibus (GEO) database (https://www.ncbi.nlm.nih.gov/geo/) under accession number GSE155360. All relevant data within the scope of the paper are publicly available.

Statistical analysis

SPSS 17.0 for Windows (IBM, Armonk, NY) and GraphPad Prism (GraphPad Software, San Diego, CA, USA) software were used for statistical analyses. Statistical evaluations were determined using Student's t test (two-tailed), Kruskal-Wallis test, or Spearman correlation test. Survival rates were calculated using the Kaplan-Meier method and comparisons were performed using the log-rank test. p value of 0.05 or less was considered as statistically significant.

SUPPLEMENTAL INFORMATION

Supplemental information can be found online at https://doi.org/10.1016/j.omto.2021.09.003.

ACKNOWLEDGMENTS

We thank all donors for sample donations. This work was supported by the grants from The National Natural Science Foundation of China (82002228, 81972007), Shandong Provincial Natural Science Foundation (ZR2020QH280), and The Key Research and Development Program of Shandong Province (2019GHZ003, 2020CXGC011304).

AUTHOR CONTRIBUTIONS

T.L. and C.W. initiated and designed the study. T.L. instructed all experiments and drafted the manuscript. P.L., J.L., Q.Q., Z.S., S.S., and S.L. conducted experiments. T.L., Y.X., Y.W., and L.D. analyzed the data. L.D. and C.W. revised the manuscript. All authors provided approval of the final manuscript.

DECLARATION OF INTERESTS

The authors declare no competing interests.

REFERENCES

1. Kayani, B., Zacharakis, E., Ahmed, K., and Hanna, G.B. (2011). Lymph node metastases and prognosis in oesophageal carcinoma–a systematic review. European journal of surgical oncology *37*, 747–753.
2. Pennathur, A., Gibson, M.K., Jobe, B.A., and Luketich, J.D. (2013). Oesophageal carcinoma. Lancet *381*, 400–412.
3. Ohashi, S., Miyamoto, S., Kikuchi, O., Goto, T., Amanuma, Y., and Muto, M. (2015). Recent Advances From Basic and Clinical Studies of Esophageal Squamous Cell Carcinoma. Gastroenterology *149*, 1700–1715.
4. Herrera, L.J. (2010). Extent of lymphadenectomy in esophageal cancer: how many lymph nodes is enough? Ann. Surg. Oncol. *17*, 676–678.
5. Chen, C., He, W., Huang, J., Wang, B., Li, H., Cai, Q., Su, F., Bi, J., Liu, H., Zhang, B., et al. (2018). LNMAT1 promotes lymphatic metastasis of bladder cancer via CCL2 dependent macrophage recruitment. Nat. Commun. *9*, 3826.
6. Wang, C., Xu, S., Tian, Y., Ju, A., Hou, Q., Liu, J., Fu, Y., and Luo, Y. (2019). Lysyl Oxidase-Like Protein 2 Promotes Tumor Lymphangiogenesis and Lymph Node Metastasis in Breast Cancer. Neoplasia *21*, 413–427.

7. Wu, H., Song, S., Yan, A., Guo, X., Chang, L., Xu, L., Hu, L., Kuang, M., Liu, B., He, D., et al. (2020). RACK1 promotes the invasive activities and lymph node metastasis of cervical cancer via galectin-1. Cancer Lett. *469*, 287–300.

8. Brown, M., Assen, F.P., Leithner, A., Abe, J., Schachner, H., Asfour, G., Bago-Horvath, Z., Stein, J.V., Uhrin, P., Sixt, M., and Kerjaschki, D. (2018). Lymph node blood vessels provide exit routes for metastatic tumor cell dissemination in mice. Science *359*, 1408–1411.

9. Bång-Rudenstam, A., Cerezo-Magaña, M., and Belting, M. (2019). Pro-metastatic functions of lipoproteins and extracellular vesicles in the acidic tumor microenvironment. Cancer Metastasis Rev. *38*, 79–92.

10. Krzystek-Korpacka, M., Matusiewicz, M., Diakowska, D., Grabowski, K., Blachut, K., and Banas, T. (2007). Up-regulation of VEGF-C secreted by cancer cells and not VEGF-A correlates with clinical evaluation of lymph node metastasis in esophageal squamous cell carcinoma (ESCC). Cancer Lett. *249*, 171–177.

11. Han, U., Can, O.I., Han, S., Kayhan, B., and Onal, B.U. (2007). Expressions of p53, VEGF C, p21: could they be used in preoperative evaluation of lymph node metastasis of esophageal squamous cell carcinoma? Dis. Esophagus *20*, 379–385.

12. Yang, Z., Wang, Y.G., and Su, K. (2015). VEGF-C and VEGF-D expression and its correlation with lymph node metastasis in esophageal squamous cell cancer tissue. Asian Pac. J. Cancer Prev. *16*, 271–274.

13. Shukla, G.C., Singh, J., and Barik, S. (2011). MicroRNAs: Processing, Maturation, Target Recognition and Regulatory Functions. Mol. Cell. Pharmacol. *3*, 83–92.

14. Calin, G.A., and Croce, C.M. (2006). MicroRNA signatures in human cancers. Nat. Rev. Cancer *6*, 857–866.

15. Han, D.L., Wang, L.L., Zhang, G.F., Yang, W.F., Chai, J., Lin, H.M., Fu, Z., and Yu, J.M. (2019). MiRNA-485-5p, inhibits esophageal cancer cells proliferation and invasion by down-regulating O-linked N-acetylglucosamine transferase. Eur. Rev. Med. Pharmacol. Sci. *23*, 2809–2816.

16. Wang, W.W., Zhao, Z.H., Wang, L., Li, P., Chen, K.S., Zhang, J.Y., Li, W.C., Jiang, G.Z., and Li, X.N. (2019). MicroRNA-134 prevents the progression of esophageal squamous cell carcinoma via the PLXNA1-mediated MAPK signalling pathway. EBioMedicine *46*, 66–78.

17. Lu, Y.F., Yu, J.R., Yang, Z., Zhu, G.X., Gao, P., Wang, H., Chen, S.Y., Zhang, J., Liu, M.Y., Niu, Y., et al. (2018). Promoter hypomethylation mediated upregulation of MicroRNA-10b-3p targets FOXO3 to promote the progression of esophageal squamous cell carcinoma (ESCC). J. Exp. Clin. Cancer Res. *37*, 301.

18. Redis, R.S., Calin, S., Yang, Y., You, M.J., and Calin, G.A. (2012). Cell-to-cell miRNA transfer: from body homeostasis to therapy. Pharmacol. Ther. *136*, 169–174.

19. Xu, R., Rai, A., Chen, M., Suwakulsiri, W., Greening, D.W., and Simpson, R.J. (2018). Extracellular vesicles in cancer - implications for future improvements in cancer care. Nat. Rev. Clin. Oncol. *15*, 617–638.

20. Zhang, Z.G., Buller, B., and Chopp, M. (2019). Exosomes - beyond stem cells for restorative therapy in stroke and neurological injury. Nat. Rev. Neurol. *15*, 193–203.

21. Fang, J.H., Zhang, Z.J., Shang, L.R., Luo, Y.W., Lin, Y.F., Yuan, Y., and Zhuang, S.M. (2018). Hepatoma cell-secreted exosomal microRNA-103 increases vascular permeability and promotes metastasis by targeting junction proteins. Hepatology *68*, 1459–1475.

22. Cheng, M., Yang, J., Zhao, X., Zhang, E., Zeng, Q., Yu, Y., Yang, L., Wu, B., Yi, G., Mao, X., et al. (2019). Circulating myocardial microRNAs from infarcted hearts are carried in exosomes and mobilise bone marrow progenitor cells. Nat. Commun. *10*, 959.

23. Xu, G., Zhang, B., Ye, J., Cao, S., Shi, J., Zhao, Y., Wang, Y., Sang, J., Yao, Y., Guan, W., et al. (2019). Exosomal miRNA-139 in cancer-associated fibroblasts inhibits gastric cancer progression by repressing MMP11 expression. Int. J. Biol. Sci. *15*, 2320–2329.

24. Mathieu, M., Martin-Jaular, L., Lavieu, G., and Théry, C. (2019). Specificities of secretion and uptake of exosomes and other extracellular vesicles for cell-to-cell communication. Nat. Cell Biol. *21*, 9–17.

25. Ji, H., Cao, R., Yang, Y., Zhang, Y., Iwamoto, H., Lim, S., Nakamura, M., Andersson, P., Wang, J., Sun, Y., et al. (2014). TNFR1 mediates TNF-α-induced tumour lymphangiogenesis and metastasis by modulating VEGF-C-VEGFR3 signalling. Nat. Commun. *5*, 4944.

26. Maeng, Y.S., Aguilar, B., Choi, S.I., and Kim, E.K. (2016). Inhibition of TGFBIp expression reduces lymphangiogenesis and tumor metastasis. Oncogene *35*, 196–205.

27. Li, L., Li, C., Wang, S., Wang, Z., Jiang, J., Wang, W., Li, X., Chen, J., Liu, K., Li, C., and Zhu, G. (2016). Exosomes Derived from Hypoxic Oral Squamous Cell Carcinoma Cells Deliver miR-21 to Normoxic Cells to Elicit a Prometastatic Phenotype. Cancer Res. *76*, 1770–1780.

28. Zhao, J., Cao, J., Zhou, L., Du, Y., Zhang, X., Yang, B., Gao, Y., Wang, Y., Ma, N., and Yang, W. (2018). MiR-1260b inhibitor enhances the chemosensitivity of colorectal cancer cells to fluorouracil by targeting PDCD4/IGF1. Oncol. Lett. *16*, 5131–5139.

29. Hiyoshi, Y., Kamohara, H., Karashima, R., Sato, N., Imamura, Y., Nagai, Y., Yoshida, N., Toyama, E., Hayashi, N., Watanabe, M., et al. (2009). MicroRNA-21 regulates the proliferation and invasion in esophageal squamous cell carcinoma. Clinical cancer research *15*, 1915–1922.

30. Sun, J., Yong, J., and Zhang, H. (2020). microRNA-93, upregulated in serum of nasopharyngeal carcinoma patients, promotes tumor cell proliferation by targeting PDCD4. Exp. Ther. Med. *19*, 2579–2587.

31. Liu, L., Lin, C., Liang, W., Wu, S., Liu, A., Wu, J., Zhang, X., Ren, P., Li, M., and Song, L. (2015). TBL1XR1 promotes lymphangiogenesis and lymphatic metastasis in esophageal squamous cell carcinoma. Gut *64*, 26–36.

32. Parikh, A.S., Puram, S.V., Faquin, W.C., Richmon, J.D., Emerick, K.S., Deschler, D.G., Varvares, M.A., Tirosh, I., Bernstein, B.E., and Lin, D.T. (2019). Immunohistochemical quantification of partial-EMT in oral cavity squamous cell carcinoma primary tumors is associated with nodal metastasis. Oral Oncol. *99*, 104458.

33. Shi, Y., Fang, N., Li, Y., Guo, Z., Jiang, W., He, Y., Ma, Z., and Chen, Y. (2020). Circular RNA LPAR3 sponges microRNA-198 to facilitate esophageal cancer migration, invasion, and metastasis. Cancer Sci. *111*, 2824–2836.

34. Ren, Z., Liu, X., Si, Y., and Yang, D. (2020). Long non-coding RNA DDX11-AS1 facilitates gastric cancer progression by regulating miR-873-5p/SPC18 axis. Artif. Cells Nanomed. Biotechnol. *48*, 572–583.

35. Fu, L., Qin, Y.R., Ming, X.Y., Zuo, X.B., Diao, Y.W., Zhang, L.Y., Ai, J., Liu, B.L., Huang, T.X., Cao, T.T., et al. (2017). RNA editing of *SLC22A3* drives early tumor invasion and metastasis in familial esophageal cancer. Proc. Natl. Acad. Sci. USA *114*, E4631–E4640.

36. Liu, T., Zhang, X., Du, L., Wang, Y., Liu, X., Tian, H., Wang, L., Li, P., Zhao, Y., Duan, W., et al. (2019). Exosome-transmitted miR-128-3p increase chemosensitivity of oxaliplatin-resistant colorectal cancer. Mol. Cancer *18*, 43.

37. Chen, Y., Knösel, T., Kristiansen, G., Pietas, A., Garber, M.E., Matsuhashi, S., Ozaki, I., and Petersen, I. (2003). Loss of PDCD4 expression in human lung cancer correlates with tumour progression and prognosis. J. Pathol. *200*, 640–646.

38. Gao, F., Zhang, P., Zhou, C., Li, J., Wang, Q., Zhu, F., Ma, C., Sun, W., and Zhang, L. (2007). Frequent loss of PDCD4 expression in human glioma: possible role in the tumorigenesis of glioma. Oncol. Rep. *17*, 123–128.

39. Wei, N.A., Liu, S.S., Leung, T.H., Tam, K.F., Liao, X.Y., Cheung, A.N., Chan, K.K., and Ngan, H.Y. (2009). Loss of Programmed cell death 4 (Pdcd4) associates with the progression of ovarian cancer. Mol. Cancer *8*, 70.

40. Fassan, M., Pizzi, M., Giacomelli, L., Mescoli, C., Ludwig, K., Pucciarelli, S., and Rugge, M. (2011). PDCD4 nuclear loss inversely correlates with miR-21 levels in colon carcinogenesis. Virchows Archiv *458*, 413–419.

41. Espadinha, A.S., Prouzet-Mauléon, V., Claverol, S., Lagarde, V., Bonneu, M., Mahon, F.X., and Cardinaud, B. (2017). A tyrosine kinase-STAT5-miR21-PDCD4 regulatory axis in chronic and acute myeloid leukemia cells. Oncotarget *8*, 76174–76188.

42. Alarcón, C.R., Lee, H., Goodarzi, H., Halberg, N., and Tavazoie, S.F. (2015). N6-methyladenosine marks primary microRNAs for processing. Nature *519*, 482–485.

43. Takahashi, R.U., Prieto-Vila, M., Hironaka, A., and Ochiya, T. (2017). The role of extracellular vesicle microRNAs in cancer biology. Clin. Chem. Lab. Med. *55*, 648–656.

44. Zhou, W., Fong, M.Y., Min, Y., Somlo, G., Liu, L., Palomares, M.R., Yu, Y., Chow, A., O'Connor, S.T., Chin, A.R., et al. (2014). Cancer-secreted miR-105 destroys vascular endothelial barriers to promote metastasis. Cancer Cell *25*, 501–515.

45. Fan, B., Jin, Y., Zhang, H., Zhao, R., Sun, M., Sun, M., Yuan, X., Wang, W., Wang, X., Chen, Z., et al. (2020). MicroRNA-21 contributes to renal cell carcinoma cell invasiveness and angiogenesis via the PDCD4/c-Jun (AP-1) signalling pathway. Int. J. Oncol. *56*, 178–192.

46. Pin, G., Huanting, L., Chengzhan, Z., Xinjuan, K., Yugong, F., Wei, L., Shifang, L., Zhaojian, L., Kun, H., Weicheng, Y., et al. (2020). Down-Regulation of PDCD4 Promotes Proliferation, Angiogenesis and Tumorigenesis in Glioma Cells. Front. Cell Dev. Biol. *8*, 593685.

47. Song, S., and Qiu, X. (2021). LncRNA miR503HG inhibits epithelial-mesenchymal transition and angiogenesis in hepatocellular carcinoma by enhancing PDCD4 via regulation of miR-15b. Digestive and liver disease *53*, 107–116.

48. Krug, S., Huth, J., Göke, F., Buchholz, M., Gress, T.M., Göke, R., and Lankat-Buttgereit, B. (2012). Knock-down of Pdcd4 stimulates angiogenesis via up-regulation of angiopoietin-2. Biochim. Biophys. Acta *1823*, 789–799.

49. Cheng, M., Sheng, L., Gao, Q., Xiong, Q., Zhang, H., Wu, M., Liang, Y., Zhu, F., Zhang, Y., Zhang, X., et al. (2019). The m^6A methyltransferase METTL3 promotes bladder cancer progression via AFF4/NF-κB/MYC signaling network. Oncogene *38*, 3667–3680.

50. Rice, T.W., Ishwaran, H., Hofstetter, W.L., Kelsen, D.P., Apperson-Hansen, C., and Blackstone, E.H.; Worldwide Esophageal Cancer Collaboration I (2016). Recommendations for pathologic staging (pTNM) of cancer of the esophagus and esophagogastric junction for the 8th edition AJCC/UICC staging manuals. In Diseases of the esophagus, *29*, pp. 897–905.

OMTO, Volume *23*

Supplemental information

Exosomal and intracellular miR-320b promotes lymphatic metastasis in esophageal squamous cell carcinoma

Tong Liu, Peilong Li, Juan Li, Qiuchen Qi, Zhaowei Sun, Shuang Shi, Yan Xie, Shibiao Liu, Yunshan Wang, Lutao Du, and Chuanxin Wang

Supplementary Materials and Methods

Antibodies and reagents

The following antibodies were used: anti-LYVE-1, Abcam (ab14917), for IHC; anti-firefly luciferase antibody, Abcam (ab185924), for IHC; anti-PDCD4, Cell Signaling Technology (#9535), for IHC and immunoblot; anti-DGCR8, Abcam (ab191875), for immunoblot, immunoprecipitation and RIP; anti- N6-methyladenosine (m6A), Abcam (ab208577), for immunoblot; anti-METTL3, Abcam (ab195352), for immunoblot and immunoprecipitation; anti-E-cadherin, Cell Signaling Technology, #73195, for immunoblot; anti-Vimentin, Cell Signaling Technology, #5741, for immunoblot; anti-GAPDH, Cell Signaling Technology, #5174, for immunoblot; Control mouse IgG, control rabbit IgG, and anti-m6A were provided in the EZ-Magna RIP kit or Magna MeRIP™ m6A Kit (Millipore). DAPI (Thermo Scientific, 62247) and PKH67 Green Fluorescent Cell Linker Mini Kit (Sigma-Aldrich, MINI67) were also used.

Lentiviral, plasmid and miRNA mimics package and cell transfection

Lentiviral plasmids encoding miR-320b overexpression, sponge and negative control were designed and produced by Wigene (Shandong, China). KYSE150 and EC9706 cells were transfected with lentivirus at a multiplicity of infection (MOI) of 20 and 20, respectively. The cells were then selected with 1μg/ml (KYSE150) or 2 μg/ml (EC9706) puromycin for 3 days. p-ENTER plasmid containing PDCD4 and negative control were purchased from Wigene. miR-320b mimics and control were produced by Biosune (Shanghai, China). Plasmid, mimics, inhibitor and negative control were transfected using (Invitrogen, California, USA) according to the manufacturer's instructions of Lipofectamine2000. The total RNA and protein were extracted after 48 hours for subsequent experiments.

Exosome purification and identification

Serum exosome extraction and cell culture medium exosome were extracted using SBI regent or ultracentrifugation as previously described [1-3]. The morphology, quantification and size distribution were analyzed using transmission electron microscopy (TEM, JEM-1-11 microscope, Japan) and ZetaView

instrument and software (Particle Metrix Ltd. Germany), respectively.

Immunohistochemistry

Immunohistochemistry was done as previously reported [3]. Positive cells were counted in five random fields per slide. Interpretation of staining intensity of anti-LYVE-1, anti-Luciferase and anti-PDCD4 was made independently by two specialists, as no staining=0, weak staining=1 (1-25%), moderate staining=2 (26-50%), and strong staining=3 (51-100%).

Luciferase reporter assay

Cells were co-transfected with Dual-Luciferase reporter system using pmiR-REPORT^{TM} luciferase vectors containing wild-type or mutant 3`-UTR of PDCD4 and miR-320b mimics or control using Lipofectamine 2000 (Invitrogen, California, USA). Luciferase activity was measured by Dual-Luciferase Reporter Assay System (Beyotime Biotechnology, Shanghai, China) 48h after transfection. Each group was run triplicate in 96-well plates.

Quantitative real-time PCR

Total RNAs were extracted from cell and exosome by the miRNeasy Micro Kit (QIAGEN, Valencia, CA, USA). RNA was reverse transcribed into cDNA using High Capacity cDNA Reverse Transcription Kit (Takara, Dalian, China). Quantitative real-time PCR was performed using Power TB Green (Takara, Dalian, China) on a CFX96 Real-Time PCR Detection System (Bio-Rad, USA). Data was collected and normalized to U6 (for cellular miR-320b), GAPDH (for cellular PDCD4 mRNA) or miR-16 (for exosomal miR-320b). MicroRNA and mRNA primers were designed and synthesized by Biosune (Shanghai, China). mRNA primers are listed in Supplementary table 2.

Immunoblotting assay

The cells were lysed using the protein extraction reagent RIPA buffer (Solarbio, China) supplemented with a protease inhibitor cocktail (Solarbio, China). Immunoblotting assay was performed as previously described [4]. Protein band was visualized using an ECL chemiluminescence kit and the intensity was quantified by

densitometry using Image Lab software (Bio-Rad, Hercules, CA, USA).

CCK-8, colony formation and EdU assays

Cells viability was determined by Cell Counting Kit 8 (Dojindo, Japan) and the optical density (OD) value was measured at 450nm wavelength with the Thermo Scientific Multiskan FC (Thermo Fisher Scientific Corporation, USA).

For the colony formation assays, 1×10^3 ESCC cells were seeded into 6-well plates and cultured for 14 days. The colonies were stained with 0.1% crystal violet and visible colonies were counted.

For EdU assays, ESCC cells were seeded in 24-well plates and incubated for 24h. Cells were stained with EdU and DAPI according to the manufacturer's instructions of the EdU kit (RioboBio, Guangzhou, China). The images were obtained with Zeiss laser scanning microscope system (Zeiss, Germany).

Cell migration and invasion assay

200μl cell suspension (2.5×10^5 cells/ml) was inoculated in the apical chamber with or without the Matrigel membrane, and the culture medium containing 20% fetal bovine serum was added to the basolateral chamber. The cells passing through the membrane in each group was stained with 0.1% crystal violet and counted by inversion microscope (Zeiss, Germany).

ELISA analysis

VEGF-C in the culture supernatants of KYSE150 cells was quantified using the Human VEGF-C Quantikine ELISA Kit (Elabscience, Wuhan, China) according to the manufacturer's protocol.

Co-immunoprecipitations assay

Co-immunoprecipitation was performed in KYSE150 cells using Co-Immunoprecipitation Kit (ThermoFisher Scientific, USA) according to the manufacturer's protocol. Briefly, immunoprecipitations of METTL3 were performed using an anti-METTL3 antibody overnight at 4°C. After washing, the immunoprecipitated complex was treated with either RNase A or RNase inhibitor (Sigma Aldrich, USA) for 5 min at 37°C. Anti-DGCR8, anti-METTL3 or anti-m6A antibody was used for immunoblot analysis.

Supplementary Table 1 Clinical characteristics

Variable, N (%)	Cohort 1			Cohort 2		
	Total	LNM (-)	LNM (+)	Total	LNM (-)	LNM (+)
Sex						
Male	128(71.9)	68(71.6)	60(72.3)	137(72.9)	61(67.0)	76(78.4)
Female	50(28.1)	27(28.4)	23(27.7)	51(27.1)	30(33.0)	21(21.6)
Age [a]						
<62	80(44.9)	46(48.4)	34(41.0)	94(50.0)	46(50.5)	48(49.5)
≥62	98(55.1)	49(51.6)	49(59.0)	94(50.0)	45(49.5)	49(50.5)
Tumor location						
Cervical-Middle thoracic	102(57.3)	49(51.6)	53(63.9)	111(59.0)	55(60.4)	56(57.7)
Low thoracic	76(42.7)	46(48.4)	30(36.1)	77(41.0)	36(39.6)	41(42.3)
Differentiation						
Well-Moderate	107(60.1)	70(73.7)	37(44.6)	105(55.8)	57(62.6)	48(49.5)
Poor	71(39.9)	25(26.3)	46(55.4)	83(44.2)	34(37.4)	49(50.5)
T stage						
T1-T2	85(47.8)	55(57.9)	30(36.1)	86(45.7)	51(56.0)	35(36.1)
T3-T4	93(52.2)	40(42.1)	53(63.9)	102(54.3)	40(44.0)	62(63.9)
Tumor size [b]						
<4.0	94(52.8)	64(67.4)	30(36.1)	95(50.5)	58(63.7)	37(38.1)
≥4.0	84(47.2)	31(32.6)	53(63.9)	93(49.5)	33(36.3)	60(61.9)
SCC level						
Normal	108(60.7)	57(60.0)	51(61.4)	122(64.9)	57(62.6)	65(67.0)
Abnormal	70(39.3)	38(40.0)	32(38.6)	66(35.1)	34(37.4)	32(33.0)
CEA level						
Normal	113(63.5)	63(66.3)	50(60.2)	126(67.0)	63(69.2)	63(64.9)
Abnormal	65(36.5)	32(33.7)	33(39.8)	62(33.0)	28(30.8)	34(35.1)
CT reported LN status						
Negative	107(60.1)	70(73.7)	37(44.6)	105(55.8)	67(73.6)	38(39.2)
Positive	71(39.9)	25(26.3)	46(55.4)	83(44.2)	24(26.4)	59(60.8)
Lymphovascular invasion						
Negative	92(51.7)	57(60.0)	35(42.2)	94(50.0)	56(61.5)	38(39.2)
Positive	86(48.3)	38(40.0)	48(57.8)	94(50.0)	35(38.5)	59(60.8)

[a] The average age was 62.

[b] Tumor size measured in longest diameter (cm), and the mean was 4.0cm.

Supplementary Table 2 Primer sequences used in this manuscript.

Primer name	Forward primer sequence	Reverse primer sequence	Application
PDCD4	AGGCAAAAAGGCGACTAAGGA	TCCAGCAACCTTCCCTTTGG	qRT-PCR
METTL3	GTGTCAGGGCTGGGAGACTA	TAGATCCAAGTGCCCCGAGT	qRT-PCR
GAPDH	GCACCGTCAAGGCTGAGAAC	TGGTGAAGACGCCAGTGGA	qRT-PCR
Pri-miR-320b	AGCTGTTAGGCAATCTCTCCTTA	CAGCAATCCTTGCTCTGAGG	qRT-PCR
Pre-miR-320b	GTCTCTTAGGCTTTCTCTTCCCAG	TTTTTCCTTTTGCCCTCTCAAC	qRT-PCR
pENTER	CGCAAATGGGCGGTAGGCGTG	CCTCTACAAATGTGGTATGGC	plasmid
PDCD4	CGCAAATGGGCGGTAGGCGTG	CCTCTACAAATGTGGTATGGC	plasmid
METTL3	CGCAAATGGGCGGTAGGCGTG	CCTCTACAAATGTGGTATGGC	plasmid
siPDCD4-1	CUGGGACUGAGGAAAUAAATT	UUUAUUUCCUCAGUCCCAGTT	siRNA
siPDCD4-2	GCCCUUAGAAGUGGAUUAATT	UUAAUCCACUUCUAAGGGCTT	siRNA
siMETTL3-1	CCUGCAAGUAUGUUCACUATT	UAGUGAACAUACUUGCAGGTT	siRNA
siMETTL3-2	GCUACCUGGACGUCAGUAUTT	AUACUGACGUCCAGGUAGCTT	siRNA
miR-320b mimics	AAAAGCUGGGUUGAGAGGGCAA	GCCCUCUCAACCCAGCUUUUUU	mimics

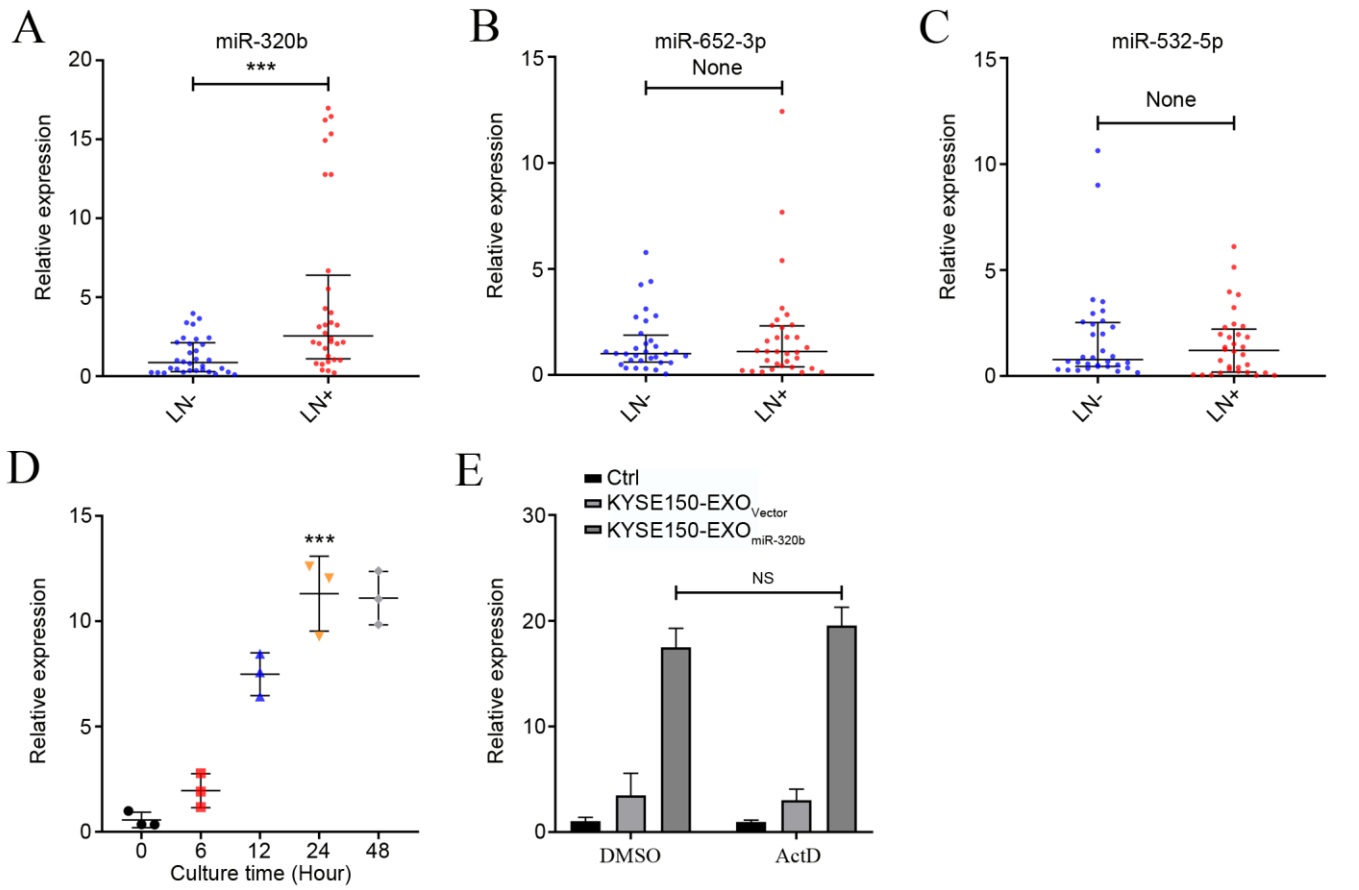

Supplementary Figure 1. Upregulation of exosomal miR-320b is associated with LN metastasis

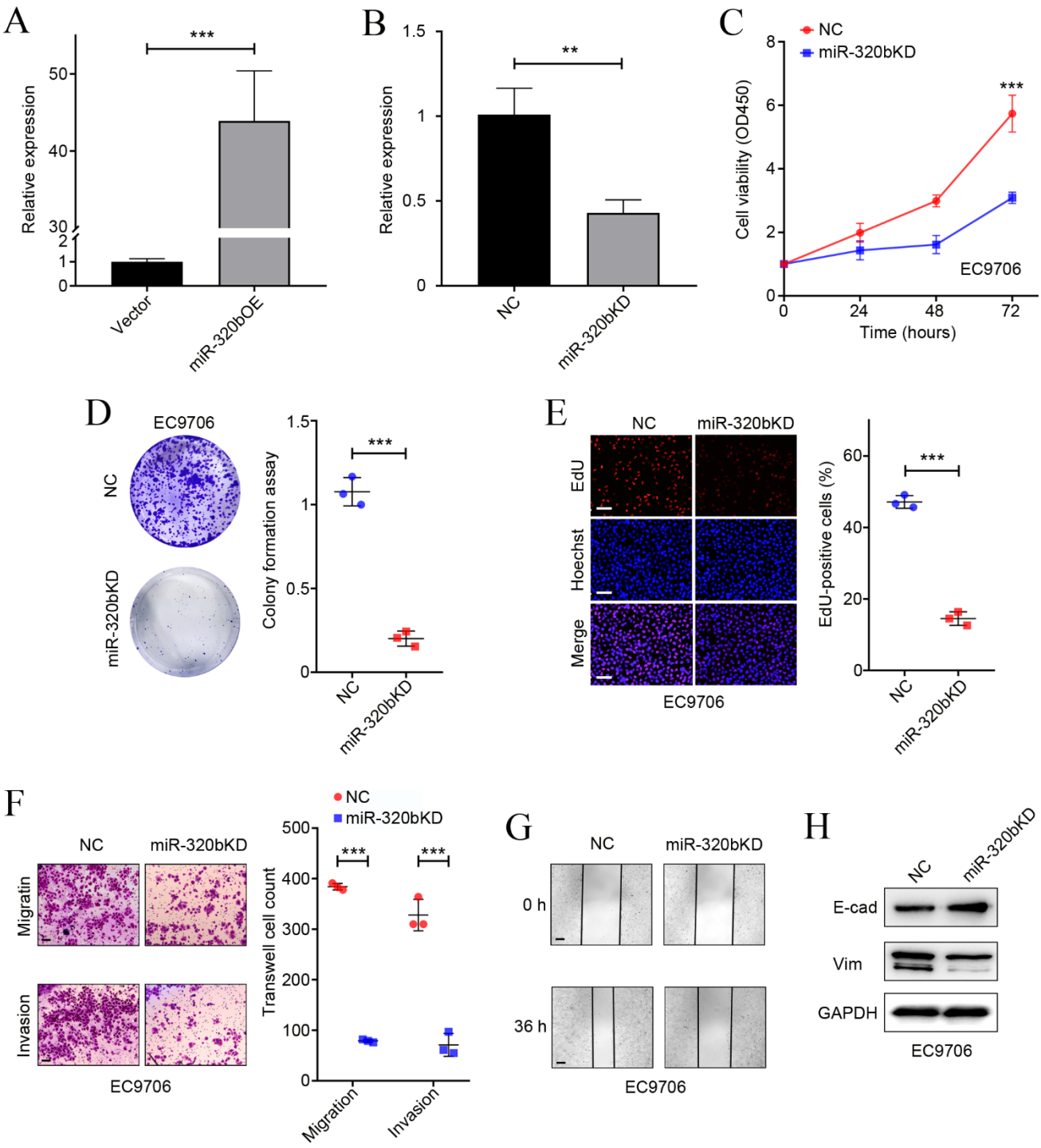

Supplementary Figure 2. miR-320b overexpression promote ESCC malignant phenotypes.

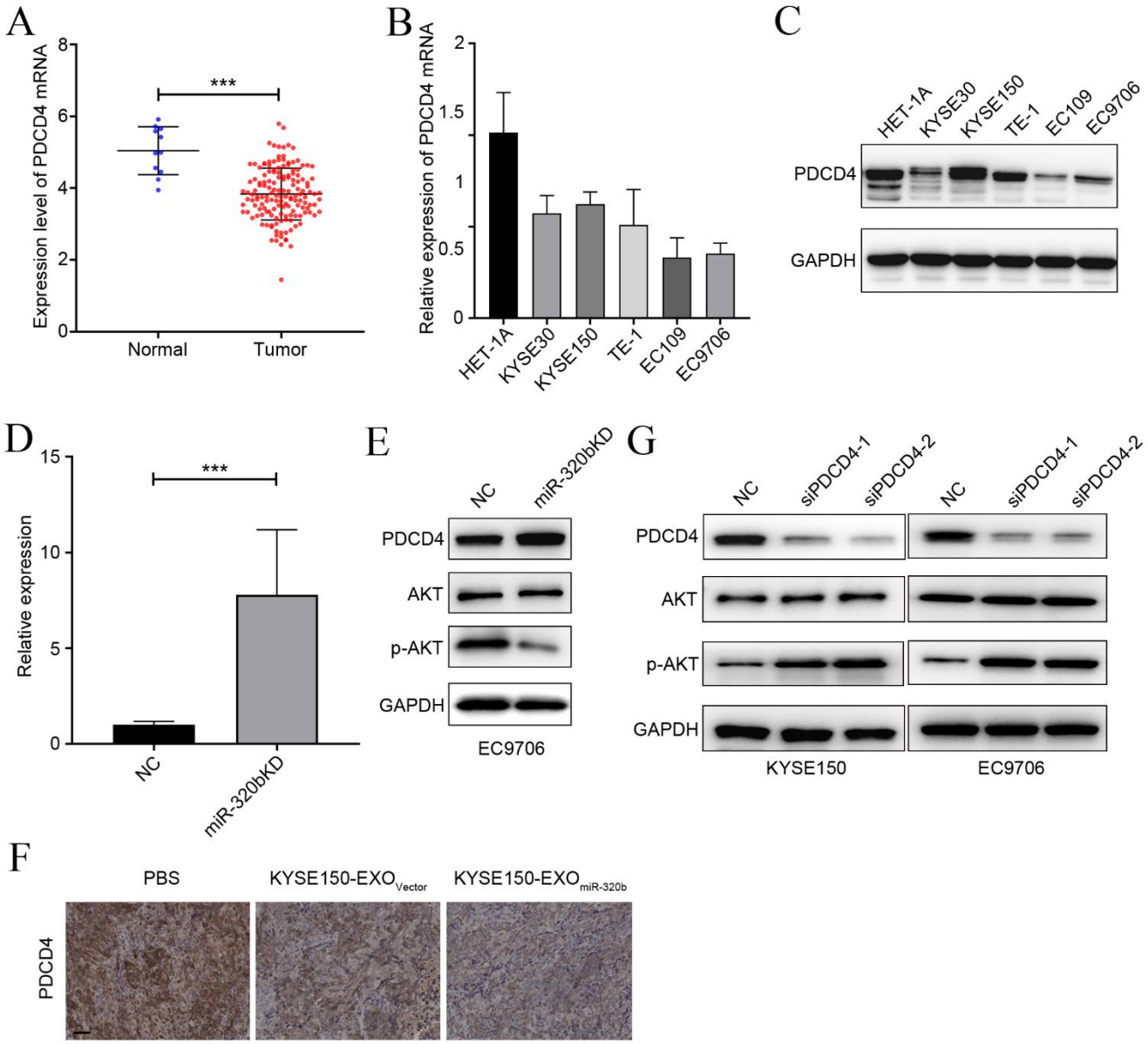

Supplementary Figure 3. Knockdown PDCD4 evokes oncogenic of ESCC cells.

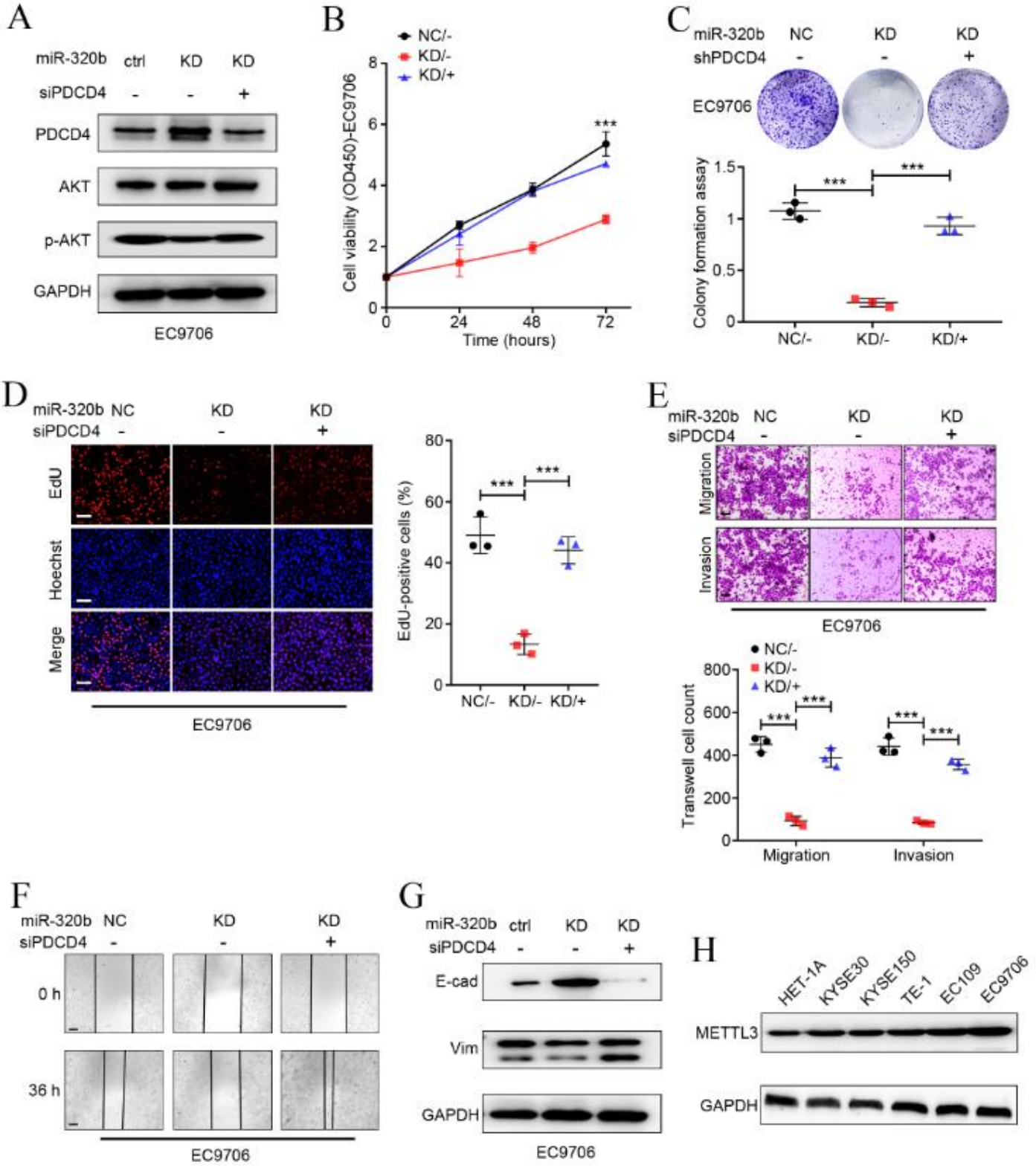

Supplementary Figure 4. miR-320b promotes ESCC cell malignant phenotypes by targeting PDCD4.

REFERENCE

1. Thery, C, Amigorena, S, Raposo, G, and Clayton, A (2006). Isolation and characterization of exosomes from cell culture supernatants and biological fluids. Current protocols in cell biology Chapter 3: Unit 3 22.

2. Liu, T, Zhang, X, Gao, S, Jing, F, Yang, Y, Du, L, et al. (2016). Exosomal long noncoding RNA CRNDE-h as a novel serum-based biomarker for diagnosis and prognosis of colorectal cancer. Oncotarget 7: 85551-85563.

3. Liu, T, Zhang, X, Du, L, Wang, Y, Liu, X, Tian, H, et al. (2019). Exosome-transmitted miR-128-3p increase chemosensitivity of oxaliplatin-resistant colorectal cancer. Molecular cancer 18: 43.

4. Li, P, Zhang, X, Wang, H, Wang, L, Liu, T, Du, L, et al. (2017). MALAT1 Is Associated with Poor Response to Oxaliplatin-Based Chemotherapy in Colorectal Cancer Patients and Promotes Chemoresistance through EZH2. Molecular cancer therapeutics 16: 739-751.